Title: Constraint-force-based approach of modelling compliant mechanisms: Principle and application

Author: Haiyang Li Guangbo Hao

PII: S0141-6359(16)30132-5
DOI: http://dx.doi.org/doi:10.1016/j.precisioneng.2016.08.001
Reference: PRE 6438

To appear in: *Precision Engineering*

Received date: 18-3-2016
Revised date: 16-7-2016
Accepted date: 2-8-2016

Please cite this article as: Li Haiyang, Hao Guangbo.Constraint-force-based approach of modelling compliant mechanisms: Principle and application.*Precision Engineering* http://dx.doi.org/10.1016/j.precisioneng.2016.08.001

Constraint-Force-Based Approach of Modelling Compliant Mechanisms: Principle and Application

Haiyang Li, Guangbo Hao*

School of Engineering-Electrical and Electronic Engineering
University College Cork, Cork, Ireland

* Corresponding author: G.Hao@ucc.ie; Tel.: +353 (0)21 4903793

Research highlights:

- A systematic approach to model compliant mechanisms is proposed.
- An XYZ compliant parallel mechanism is modelled using the proposed approach.
- FEA simulations and experimental tests are conducted.

Abstract

Numerous works have been conducted on modelling basic compliant elements such as wire beams, and closed-form analytical models of most basic compliant elements have been well developed. However, the modelling of complex compliant mechanisms is still a challenging work. This paper proposes a constraint-force-based (CFB) modelling approach to model compliant mechanisms with a particular emphasis on modelling complex compliant mechanisms. The proposed CFB modelling approach can be regarded as an improved free-body-diagram (FBD) based modelling approach, and can be extended to a development of the screw-theory-based design approach. A compliant mechanism can be decomposed into rigid stages and compliant modules. A compliant module can offer elastic forces due to its deformation. Such elastic forces are regarded as variable constraint forces in the CFB modelling approach. Additionally, the CFB modelling approach defines external forces applied on a compliant mechanism as constant constraint forces. If a compliant mechanism is at static equilibrium, all the rigid stages are also at static equilibrium under the influence of the variable and constant constraint forces. Therefore, the constraint force equilibrium equations for all the rigid stages can be obtained, and the analytical model of the compliant mechanism can be derived based on the constraint force equilibrium equations. The CFB modelling approach can model a compliant mechanism linearly and nonlinearly, can obtain displacements of any points of the rigid stages, and allows external forces to be exerted on any positions of the rigid stages. Compared with the FBD based modelling approach, the CFB modelling approach does not need to identify the possible deformed configuration of a complex compliant mechanism to obtain the geometric compatibility conditions and the force equilibrium equations. Additionally, the mathematical expressions in the CFB approach have an easily understood physical meaning. Using the CFB modelling approach, the variable constraint forces of three compliant modules, a wire beam, a four-beam compliant module and an eight-beam compliant module, have been derived in this paper. Based on these variable constraint forces, the linear and non-linear models of a decoupled XYZ compliant parallel mechanism are derived, and verified by FEA simulations and experimental tests.

1 Introduction

Compliant mechanisms have no traditional sliding and rolling joints, and they transmit or transform displacements, forces and energy by means of the elastic deformations of their compliant members [1-7]. Compared with traditional rigid-body mechanisms, compliant mechanisms have the following main advantages: reduced number of parts, decreased assembly requirements, reduced product weight, no friction, no need for lubrication and no backlash [1-7]. Therefore, they are gaining more and more attention in a variety of applications such as micro- and nano-manipulation, high precision alignment, MEMS sensors and actuators, energy harvesting, medical devices, adjustable mounting and consumer products [8-14].

In order to obtain relationships between geometric parameters and motion characteristics (such as cross-axis coupling, parasitic motion, lost motion and drive stiffness) of a compliant mechanism to offer design insights, it is essential to obtain the analytical model of the compliant mechanism [14, 15]. Numerous works have been conducted on modelling compliant mechanisms [5, 15-26]. There are two main approaches of dealing with such modelling: one is the free-body-diagram (FBD) based modelling approach [16], the other is the energy-based approach using virtual work principle [27]. Compared with the FBD based modelling approach, the energy-based approach can simplify modelling process of compliant mechanisms through ignoring some internal variables, but the ignored internal variables may be needed to estimate the motion characteristics of the compliant mechanisms [28]. Awtar [29] also claimed that it was very difficult to derive an inverse relationship using the energy based approach. Therefore, the basic principle of the FBD based modelling approach is followed in this paper.

This paper proposes a constraint-force-based (CFB) approach of modelling compliant mechanisms, which can be regarded as a development of the FBD based modelling approach. The proposed CFB modelling approach can model a compliant mechanism linearly and nonlinearly, with consideration of all applied external forces. Compared with the FBD based modelling approach, the CFB modelling approach does not need to identify the possible deformed configuration of a compliant mechanism to obtain the geometric compatibility conditions and the force equilibrium equations. Moreover, the mathematical expression in the CFB modelling approach has an easily understood physical meaning.

In the CFB modelling approach, a compliant mechanism is decomposed into rigid stages and compliant modules [30, 31], and the compliant modules are regarded as multi-DOF (degree of freedom) or multi-DOC (degree of constraint) springs. A deformed compliant module stores potential energy which can offer elastic forces to the connected rigid stages. Such elastic forces are termed *variable constraint forces* in this paper, because the elastic forces vary with the deformation of the compliant modules. Additionally, this paper regards the external forces exerted on a compliant mechanism as *constant constraint forces*, because the external forces are independent of the deformation of the compliant mechanisms. If a compliant mechanism is at static equilibrium, the rigid stages are at static equilibrium under the influence of the variable constraint forces and the applied constant constraint

forces. Therefore, the constraint force equilibrium equations for the rigid stages can be represented by the associated variable and constant constraint forces. The analytical model of the compliant mechanism can be further derived based on the constraint force equilibrium equations.

In this paper, compliant modules are divided into two types, basic compliant modules and non-basic compliant modules. If a compliant module contains only one basic compliant element, the compliant module is a basic compliant module; otherwise, the compliant module is a non-basic compliant module. A wire beam, a sheet beam, a short beam, a notch hinge and a split tube are basic compliant modules [32]. A non-basic compliant module is composed of several basic compliant modules in a serial, parallel or hybrid configuration. The variable constraint force of a basic compliant module can be derived from its force-displacement relationship. Note that this paper does not consider how to obtain force-displacement relationships of basic compliant modules. The variable constraint force of a non-basic compliant module can also be derived from the force-displacement relationship of the non-basic compliant module, if this force-displacement relationship is already known. If the force-displacement relationship of the non-basic compliant module is not known, the non-basic compliant module should be further decomposed into basic compliant modules or other non-basic compliant modules whose force-displacement relationships are known. Taking the XYZ compliant parallel mechanism (CPM) shown in Fig. 1(a) that is proposed in [17] for example, the XYZ CPM can be decomposed into three effective non-basic compliant modules, Leg-X, Leg-Y and Leg-Z, as shown in Fig. 1(b). Each of the legs can also be decomposed into an actuated module (AM) and a passive module (PM), as shown in Fig. 1(c). It can be seen from Fig. 1(c) that the AM and PM can also be further decomposed into basic compliant modules, wire beams. The variable constraint forces of Leg-X, Leg-Y and Leg-Z can be obtained from their own force-displacement relationships, or derived based on the variable constraint forces of the AMs and PMs. The variable constraint forces of the AM and PM can be obtained from their own force-displacement relationships, or derived based on the variable constraint forces of the wire beams.

The variable constraint forces and the constant constraint forces, in the CFB modelling approach, are all represented by wrenches in the screw theory, which may extend the CFB modelling approach to a development of the screw-theory-based design approach reported in [33]. In the screw-theory-based design approach, compliant modules are regarded as constraints represented by wrenches [33-38]. The wrenches can represent the directions and positions of the constraints of the compliant modules, while the exact values of constraint forces are not taken into account. In other words, the screw-theory-based design approach is actually the method of arranging the directions and positions of compliant modules under the design requirements. In the screw-theory-based design approach, the constraint force provided by a compliant module is always represented by binary number zero or one [30]. A constraint force equals zero if the associated direction is a DOF direction; otherwise equals one. However, the CFB modelling approach not only takes the direction and position of the constraint of a compliant module into account, but also represents the exact constraint forces produced by the compliant module. Therefore, a compliant mechanism with specific characteristics can be designed through arranging the associated compliant modules using the CFB modelling approach, based on the variable constraint forces produced by the compliant modules. It is well known that the freedom and constraint topology (FACT) approach also offers a set of geometric entities which describe the possible permitted directions and positions of compliant modules for designing compliant mechanisms [39-41]. Compliant modules in the CFB modelling approach can be basic and non-basic compliant modules, while compliant modules in the FACT approach are mainly basic wire beams. Therefore, an appropriate process of designing a compliant mechanism can be to design the non-basic compliant modules using the FACT approach, and to arrange the directions and positions of the non-basic compliant modules in the compliant mechanism using the CFB modelling approach.

The CFB modelling approach can be used to model any compliant mechanisms. Without loss of generality, the compact and decoupled XYZ CPM shown in Fig. 1(a) is modelled using the CFB modelling approach in this paper. This XYZ CPM can be decomposed into two types of non-basic compliant modules (AMs and PMs, as shown in Fig. 1(c)), and the basic compliant module of the non-basic compliant modules is a wire beam with uniformed cross section. In this paper, the variable constraint force of the wire beam is derived first from its force-displacement relationship. Furthermore, the variable constraint forces of the two types of non-basic compliant modules are obtained based on the variable constraint force of the wire beam. Finally, the analytical model of the XYZ CPM is obtained using the derived variable constraint forces of the non-basic compliant modules. The modelling of the XYZ CPM not only shows the procedure of the CFB modelling approach, but also demonstrates the derivation of variable constraint forces of basic and non-basic compliant modules. Therefore, following the process of this modelling example, any other compliant mechanisms can be modelled using the CFB modelling approach. In addition, the derived analytical model of the XYZ CPM is also verified by FEA simulations and experimental tests.

The remainder of this paper is organized as follows. Section 2 reviews the background theories. The variable constraint force of a basic compliant module, a wire beam, is derived based on the force-displacement relationship in Section 3. The CFB modelling approach is proposed in Section 4, followed by case studies in Section 5. The FEA and experimental tests are carried out in Section 6. Finally, the conclusions are drawn in Section 7. Note that constraint forces (variable constraint forces and constant constraint forces) can also be classified into translational constraint forces and rotational constraint forces. In this paper, the translational constraint forces are normalized by EI/L^2, and the rotational constraint forces are normalized by EI/L. Here E is the Young's modulus, I is the moment of inertia of cross-section area of a beam, and L is the beam's length. In addition, all parameters in terms of geometric length are normalized by the beam's length L.

2 Constraint Forces in Screw Theory

A constraint force can be represented by a screw vector termed a wrench [33]. A wrench can also be represented as a wrench line, with location, orientation and pitch, where the pitch refers to the coupling between the translational constraint force and the rotational constraint force. A translational constraint force can restrict all translations along the wrench line in the two possible opposite directions, and a rotational constraint force can restrict all rotations about the wrench line in the two possible opposite directions. Therefore, a constraint force can be represented by a wrench, as written in Eq. (1) [35].

$$\boldsymbol{\zeta}=\begin{bmatrix}\boldsymbol{fj}\\ \boldsymbol{\tau j}\end{bmatrix}=\begin{cases}\begin{bmatrix}\boldsymbol{fj} & \boldsymbol{r}\times\boldsymbol{fj}+q\boldsymbol{fj}\end{bmatrix}^{\mathrm{T}} & \text{force and moment}\\ \begin{bmatrix}\boldsymbol{fj} & \boldsymbol{r}\times\boldsymbol{fj}\end{bmatrix}^{\mathrm{T}} & q=0,\text{ pure force}\\ \begin{bmatrix}\boldsymbol{0} & \boldsymbol{\tau j}\end{bmatrix}^{\mathrm{T}} & q\to\infty,\text{ pure moment}\end{cases} \tag{1}$$

where $\boldsymbol{\zeta}$ is a wrench. $\boldsymbol{f}$ and $\boldsymbol{\tau}$ are two three-dimensional vectors which represent translational and rotational constraint forces, respectively. $\boldsymbol{r}$ is a location vector which points from the origin of the coordinate system to a point on the wrench line. The pitch is defined by $q=(\boldsymbol{f}\cdot\boldsymbol{\tau})/(\boldsymbol{f}\cdot\boldsymbol{f})$. Here j, termed *direction coefficient*, equals ±1, which indicates the two possible opposite directions of a wrench.

In a coordinate system O-XYZ, the unit wrenches along and about the three axes are defined as principal wrenches [33, 34], which are shown in Eq. (2) and Fig. 2(a). Each of the unit wrenches is along or about one of the six directions in the coordinate system, and the magnitude of the unit wrench is one.

$$\boldsymbol{\zeta}_{\mathrm{tx}}=[j_{\mathrm{tx}},0,0,0,0,0]^{\mathrm{T}},\boldsymbol{\zeta}_{\mathrm{ty}}=\begin{bmatrix}0,j_{\mathrm{ty}},0,0,0,0\end{bmatrix}^{\mathrm{T}},\boldsymbol{\zeta}_{\mathrm{tz}}=\begin{bmatrix}0,0,j_{\mathrm{tz}},0,0,0\end{bmatrix}^{\mathrm{T}},\boldsymbol{\zeta}_{\mathrm{rx}}=\begin{bmatrix}0,0,0,j_{\mathrm{rx}},0,0\end{bmatrix}^{\mathrm{T}},\boldsymbol{\zeta}_{\mathrm{ry}}=\begin{bmatrix}0,0,0,0,j_{\mathrm{ry}},0\end{bmatrix}^{\mathrm{T}},\boldsymbol{\zeta}_{\mathrm{rz}}=\begin{bmatrix}0,0,0,0,0,j_{\mathrm{rz}}\end{bmatrix}^{\mathrm{T}} \tag{2}$$

where the subscripts tx, ty and tz indicate the translations along X-, Y- and Z-axes, and the subscripts rx, ry and rz indicate the rotations about X-, Y- and Z-axes, respectively. The non-zero element in each of the principal wrenches equals ±1, which represents the two possible opposite directions of the principal wrench.

Any one wrench can be demonstrated as a specific combination of the principal wrenches, as illustrated in Eq. (3) and Fig. 2(b) [42].

$$\boldsymbol{\zeta}=k_{\mathrm{tx}}\boldsymbol{\zeta}_{\mathrm{tx}}+k_{\mathrm{ty}}\boldsymbol{\zeta}_{\mathrm{ty}}+k_{\mathrm{tz}}\boldsymbol{\zeta}_{\mathrm{tz}}+k_{\mathrm{rx}}\boldsymbol{\zeta}_{\mathrm{rx}}+k_{\mathrm{ry}}\boldsymbol{\zeta}_{\mathrm{ry}}+k_{\mathrm{rz}}\boldsymbol{\zeta}_{\mathrm{rz}}=\begin{bmatrix}k_{\mathrm{tx}}j_{\mathrm{tx}},k_{\mathrm{ty}}j_{\mathrm{ty}},k_{\mathrm{tz}}j_{\mathrm{tz}},k_{\mathrm{rx}}j_{\mathrm{rx}},k_{\mathrm{ry}}j_{\mathrm{ry}},k_{\mathrm{rz}}j_{\mathrm{rz}}\end{bmatrix}^{\mathrm{T}} \tag{3}$$

where k_{tx}, k_{ty}, k_{tz}, k_{rx}, k_{ry} and k_{rz} are *constraint coefficients*, which are defined in [30]. When using Eq. (3) to represent only directions of DOC and DOF, a constraint coefficient equals one if the associated constraint is infinitely large, but equals zero if the associated constraint is infinitely small. In other words, if a constraint coefficient equals one, the direction associated with the constraint coefficient is a DOC direction; otherwise it is a DOF direction. However, if using Eq. (3) to illustrate the exact constraint forces produced by a compliant module, the constraint coefficients should be assigned exact values [42]. Additionally, j_{tx}, j_{ty}, j_{tz}, j_{rx}, j_{ry} and j_{rz} are direction coefficients.

3 Variable Constraint Force of Basic Compliant Module

As mentioned in Section 1, in order to use the proposed CFB modelling approach to model a complex compliant mechanism, the variable constraint forces of the associated basic compliant modules of the complex compliant mechanism should be obtained first, based on the force-displacement relationships of the basic compliant modules. In this section, the variable constraint force of a basic compliant module, a wire beam with uniformed cross section as shown in Fig. 3, is derived from its force-displacement relationship.

Suppose that wrench $\boldsymbol{\zeta}_{\mathrm{b}}$ represents the variable constraint force of the wire beam in the coordinate system O_b-$X_bY_bZ_b$. A displacement vector, $\boldsymbol{\xi}_{\mathrm{b}}$, is used to indicate the displacements of the beam's free tip center along and about the three axes of the coordinate system [33, 43]. The wrench $\boldsymbol{\zeta}_{\mathrm{b}}$ and the displacement vector $\boldsymbol{\xi}_{\mathrm{b}}$ can be written as below.

$$\begin{aligned}\boldsymbol{\zeta}_{\mathrm{b}}&=k_{\mathrm{ob\text{-}tx}}\boldsymbol{\zeta}_{\mathrm{ob\text{-}tx}}+k_{\mathrm{ob\text{-}ty}}\boldsymbol{\zeta}_{\mathrm{ob\text{-}ty}}+k_{\mathrm{ob\text{-}tz}}\boldsymbol{\zeta}_{\mathrm{ob\text{-}tz}}+k_{\mathrm{ob\text{-}rx}}\boldsymbol{\zeta}_{\mathrm{ob\text{-}rx}}+k_{\mathrm{ob\text{-}ry}}\boldsymbol{\zeta}_{\mathrm{ob\text{-}ry}}+k_{\mathrm{ob\text{-}rz}}\boldsymbol{\zeta}_{\mathrm{ob\text{-}rz}}\\ &=\begin{bmatrix}k_{\mathrm{ob\text{-}tx}}j_{\mathrm{ob\text{-}tx}},k_{\mathrm{ob\text{-}ty}}j_{\mathrm{ob\text{-}ty}},k_{\mathrm{ob\text{-}tz}}j_{\mathrm{ob\text{-}tz}},k_{\mathrm{ob\text{-}rx}}j_{\mathrm{ob\text{-}rx}},k_{\mathrm{ob\text{-}ry}}j_{\mathrm{ob\text{-}ry}},k_{\mathrm{ob\text{-}rz}}j_{\mathrm{ob\text{-}rz}}\end{bmatrix}^{\mathrm{T}}\\ &=\begin{bmatrix}\zeta_{\mathrm{b\text{-}tx}},\zeta_{\mathrm{b\text{-}ty}},\zeta_{\mathrm{b\text{-}tz}},\zeta_{\mathrm{b\text{-}rx}},\zeta_{\mathrm{b\text{-}ry}},\zeta_{\mathrm{b\text{-}rz}}\end{bmatrix}^{\mathrm{T}}\end{aligned} \tag{4}$$

$$\boldsymbol{\xi}_{\mathrm{b}}=\begin{bmatrix}\xi_{\mathrm{b\text{-}tx}},\xi_{\mathrm{b\text{-}ty}},\xi_{\mathrm{b\text{-}tz}},\xi_{\mathrm{b\text{-}rx}},\xi_{\mathrm{b\text{-}ry}},\xi_{\mathrm{b\text{-}rz}}\end{bmatrix}^{\mathrm{T}} \tag{5}$$

where $\zeta_{\mathrm{b\text{-}tx}}$, $\zeta_{\mathrm{b\text{-}ty}}$, $\zeta_{\mathrm{b\text{-}tz}}$, $\zeta_{\mathrm{b\text{-}rx}}$, $\zeta_{\mathrm{b\text{-}ry}}$ and $\zeta_{\mathrm{b\text{-}rz}}$ are the components of the wrench $\boldsymbol{\zeta}_{\mathrm{b}}$, which represent the variable constraint forces along and about the X_b-, Y_b- and Z_b-axes of the coordinate system O_b-$X_bY_bZ_b$, respectively. $k_{\mathrm{ob\text{-}tx}}$, $k_{\mathrm{ob\text{-}ty}}$, $k_{\mathrm{ob\text{-}tz}}$, $k_{\mathrm{ob\text{-}rx}}$, $k_{\mathrm{ob\text{-}ry}}$ and $k_{\mathrm{ob\text{-}rz}}$ are the constraint coefficients, $\boldsymbol{\zeta}_{\mathrm{ob\text{-}tx}}$, $\boldsymbol{\zeta}_{\mathrm{ob\text{-}ty}}$, $\boldsymbol{\zeta}_{\mathrm{ob\text{-}tz}}$, $\boldsymbol{\zeta}_{\mathrm{ob\text{-}rx}}$, $\boldsymbol{\zeta}_{\mathrm{ob\text{-}ry}}$ and $\boldsymbol{\zeta}_{\mathrm{ob\text{-}rz}}$ are the principal wrenches of the coordinate system O_b-$X_bY_bZ_b$, and $j_{\mathrm{ob\text{-}tx}}$, $j_{\mathrm{ob\text{-}ty}}$, $j_{\mathrm{ob\text{-}tz}}$, $j_{\mathrm{ob\text{-}rx}}$, $j_{\mathrm{ob\text{-}ry}}$ and $j_{\mathrm{ob\text{-}rz}}$ are the direction coefficients. $\xi_{\mathrm{b\text{-}tx}}$, $\xi_{\mathrm{b\text{-}ty}}$, $\xi_{\mathrm{b\text{-}tz}}$, $\xi_{\mathrm{b\text{-}rx}}$, $\xi_{\mathrm{b\text{-}ry}}$ and $\xi_{\mathrm{b\text{-}rz}}$ are the displacements of the beam's free tip center along and about the three axes of the coordinate system O_b-$X_bY_bZ_b$.

If the displacement of a beam's free tip center is $\boldsymbol{\xi}_{\mathrm{b}}$, due to the influence of an applied force $\boldsymbol{\zeta}_{\mathrm{bf}}$, the relationship between the $\boldsymbol{\xi}_{\mathrm{b}}$ and the $\boldsymbol{\zeta}_{\mathrm{bf}}$ is the force-displacement relationship of the beam. The nonlinear force-displacement relationship of a wire beam has been developed in [27], which is very accurate (for medium motion ranges, i.e., deflection is less than 0.1% of wire beam's length) but complicated. When the rotations of a wire beam are much smaller than the translations, a simplified force-displacement relationship of the wire beam has been proposed in [18]. The simplified force-displacement relationship proposed in [18] is

adopted in this paper, therefore, the derived variable constraint force of a wire beam is valid for modelling translational compliant mechanisms. The simplified force-displacement relationship is rewritten, as shown in Eq. (6).

$$\xi_{\text{b-tx}}=\begin{pmatrix}\dfrac{\zeta_{\text{bf-tx}}t_{\text{b}}^{\,2}}{12}+\xi_{\text{b-rz}}\left(\dfrac{\xi_{\text{b-ty}}}{20}-\dfrac{\xi_{\text{b-rz}}}{15}\right)+\left(\dfrac{\xi_{\text{b-rz}}}{20}-\dfrac{3\xi_{\text{b-ty}}}{5}\right)\xi_{\text{b-ty}}+\xi_{\text{b-rz}}\left(\dfrac{11\zeta_{\text{bf-tx}}\xi_{\text{b-rz}}}{6300}-\dfrac{\zeta_{\text{bf-tx}}\xi_{\text{b-ty}}}{1400}\right)+\xi_{\text{b-ty}}\left(\dfrac{\zeta_{\text{bf-tx}}\xi_{\text{b-ty}}}{700}-\dfrac{\zeta_{\text{bf-tx}}\xi_{\text{b-rz}}}{1400}\right)+\xi_{\text{b-rz}}\left(\dfrac{\zeta_{\text{bf-tx}}^2\xi_{\text{b-rz}}}{18000}-\dfrac{\zeta_{\text{bf-tx}}^2\xi_{\text{b-ty}}}{84000}\right)\\+\xi_{\text{b-ty}}\left(\dfrac{\zeta_{\text{bf-tx}}^2\xi_{\text{b-ty}}}{42000}-\dfrac{\zeta_{\text{bf-tx}}^2\xi_{\text{b-rz}}}{84000}\right)-\xi_{\text{b-ry}}\left(\dfrac{\xi_{\text{b-ry}}}{15}+\dfrac{\xi_{\text{b-tz}}}{20}\right)+\left(-\dfrac{\xi_{\text{b-ry}}}{20}-\dfrac{3\xi_{\text{b-tz}}}{5}\right)\xi_{\text{b-tz}}-\xi_{\text{b-ry}}\left(-\dfrac{11\zeta_{\text{bf-tx}}\xi_{\text{b-ry}}}{6300}-\dfrac{\zeta_{\text{bf-tx}}\xi_{\text{b-tz}}}{1400}\right)+\xi_{\text{b-tz}}\left(\dfrac{\zeta_{\text{bf-tx}}\xi_{\text{b-ry}}}{1400}+\dfrac{\zeta_{\text{bf-tx}}\xi_{\text{b-tz}}}{700}\right)\\-\xi_{\text{b-ry}}\left(-\dfrac{\xi_{\text{b-ry}}\zeta_{\text{bf-tx}}^2}{18000}-\dfrac{\xi_{\text{b-tz}}\zeta_{\text{bf-tx}}^2}{84000}\right)+\xi_{\text{b-tz}}\left(\dfrac{\xi_{\text{b-ry}}\zeta_{\text{bf-tx}}^2}{84000}+\dfrac{\xi_{\text{b-tz}}\zeta_{\text{bf-tx}}^2}{42000}\right)\end{pmatrix} \tag{6a}$$

$$\zeta_{\text{bf-ty}}=\frac{\xi_{\text{b-rz}}\zeta_{\text{bf-tx}}^2}{1400}-\frac{1}{700}\xi_{\text{b-ty}}\zeta_{\text{bf-tx}}^2-\frac{\xi_{\text{b-rz}}\zeta_{\text{bf-tx}}}{10}+\frac{6\xi_{\text{b-ty}}\zeta_{\text{bf-tx}}}{5}-6\xi_{\text{b-rz}}+12\xi_{\text{b-ty}} \tag{6b}$$

$$\zeta_{\text{bf-tz}}=-\frac{\xi_{\text{b-ry}}\zeta_{\text{bf-tx}}^2}{1400}-\frac{1}{700}\xi_{\text{b-tz}}\zeta_{\text{bf-tx}}^2+\frac{\xi_{\text{b-ry}}\zeta_{\text{bf-tx}}}{10}+\frac{6\xi_{\text{b-tz}}\zeta_{\text{bf-tx}}}{5}+6\xi_{\text{b-ry}}+12\xi_{\text{b-tz}} \tag{6c}$$

$$\xi_{\text{b-rx}}=\frac{\zeta_{\text{bf-rx}}}{\delta_{\text{b}}}+\frac{\zeta_{\text{bf-tx}}\left(\xi_{\text{ry}}\xi_{\text{ty}}+\xi_{\text{rz}}\xi_{\text{tz}}\right)}{10\delta_{\text{b}}}+\frac{6\left(\xi_{\text{ry}}\xi_{\text{ty}}+\xi_{\text{rz}}\xi_{\text{tz}}\right)}{\delta_{\text{b}}} \tag{6d}$$

$$-\zeta_{\text{bf-ry}}=\frac{11\xi_{\text{b-ry}}\zeta_{\text{bf-tx}}^2}{6300}+\frac{\xi_{\text{b-tz}}\zeta_{\text{bf-tx}}^2}{1400}-\frac{2\xi_{\text{b-ry}}\zeta_{\text{bf-tx}}}{15}-\frac{\xi_{\text{b-tz}}\zeta_{\text{bf-tx}}}{10}-4\xi_{\text{b-ry}}-6\xi_{\text{b-tz}} \tag{6e}$$

$$\zeta_{\text{bf-rz}}=-\frac{11\xi_{\text{b-rz}}\zeta_{\text{bf-tx}}^2}{6300}+\frac{\xi_{\text{b-ty}}\zeta_{\text{bf-tx}}^2}{1400}+\frac{2\xi_{\text{b-rz}}\zeta_{\text{bf-tx}}}{15}-\frac{\xi_{\text{b-ty}}\zeta_{\text{bf-tx}}}{10}+4\xi_{\text{b-rz}}-6\xi_{\text{b-ty}} \tag{6f}$$

where t_{b} is the thickness of the beam (square cross section). $\delta_{\text{b}}\approx 0.84375/(1+\upsilon_{\text{b}})$, here υ_{b} is the Poisson's ratio of the material. $\zeta_{\text{fb-tx}}$, $\zeta_{\text{fb-ty}}$, $\zeta_{\text{fb-tz}}$, $\zeta_{\text{fb-rx}}$, $\zeta_{\text{fb-ry}}$ and $\zeta_{\text{fb-rz}}$ are the components of the force vector $\boldsymbol{\zeta}_{\text{fb}}$, which represent the forces along and about the X_{b}-, Y_{b}- and Z_{b}-axes of the coordinate system O_{b}-$X_{\text{b}}Y_{\text{b}}Z_{\text{b}}$, respectively. It can be seen from Eq. (6) that the applied force vector $\boldsymbol{\zeta}_{\text{bf}}$ is the function of the t_{b}, δ_{b} and the entries of the displacement vector $\boldsymbol{\xi}_{\text{b}}$. So the force vector $\boldsymbol{\zeta}_{\text{bf}}$ can be written as

$$\boldsymbol{\zeta}_{\text{bf}}=\mathrm{K}_{\text{Beam}}\left(\boldsymbol{\xi}_{\text{b}},t_{\text{b}},\delta_{\text{b}}\right)=\left[\mathrm{K}_{\text{B-tx}}\left(\boldsymbol{\xi}_{\text{b}},t_{\text{b}},\delta_{\text{b}}\right),\mathrm{K}_{\text{B-ty}}\left(\boldsymbol{\xi}_{\text{b}},t_{\text{b}},\delta_{\text{b}}\right),\mathrm{K}_{\text{B-tz}}\left(\boldsymbol{\xi}_{\text{b}},t_{\text{b}},\delta_{\text{b}}\right),\mathrm{K}_{\text{B-rx}}\left(\boldsymbol{\xi}_{\text{b}},t_{\text{b}},\delta_{\text{b}}\right),\mathrm{K}_{\text{B-ry}}\left(\boldsymbol{\xi}_{\text{b}},t_{\text{b}},\delta_{\text{b}}\right),\mathrm{K}_{\text{B-rz}}\left(\boldsymbol{\xi}_{\text{b}},t_{\text{b}},\delta_{\text{b}}\right)\right]^{\text{T}} \tag{7}$$

where $\mathrm{K}_{\text{Beam}}(\cdot)$ is a 6×1 variable matrix (vector), whose components are six functions, $\mathrm{K}_{\text{B-tx}}(\cdot)$, $\mathrm{K}_{\text{B-ty}}(\cdot)$, $\mathrm{K}_{\text{B-tz}}(\cdot)$, $\mathrm{K}_{\text{B-rx}}(\cdot)$, $\mathrm{K}_{\text{B-ry}}(\cdot)$ and $\mathrm{K}_{\text{B-rz}}(\cdot)$. The six functions can be obtained based on Eq. (6), so that the values of the six functions are $\zeta_{\text{fb-tx}}$, $\zeta_{\text{fb-ty}}$, $\zeta_{\text{fb-tz}}$, $\zeta_{\text{fb-rx}}$, $\zeta_{\text{fb-ry}}$ and $\zeta_{\text{fb-rz}}$, respectively. When the beam is at a static equilibrium status, the wrench $\boldsymbol{\zeta}_{\text{b}}$ is the reaction force of $\boldsymbol{\zeta}_{\text{bf}}$. According to Newton's third law, it can be derived that $\boldsymbol{\zeta}_{\text{b}}=-\boldsymbol{\zeta}_{\text{bf}}$. Therefore, the wrench $\boldsymbol{\zeta}_{\text{b}}$ can be written as

$$\boldsymbol{\zeta}_{\text{b}}=-\mathrm{K}_{\text{Beam}}\left(\boldsymbol{\xi}_{\text{b}},t_{\text{b}},\delta_{\text{b}}\right) \tag{8}$$

Suppose that all rotational displacement components in $\boldsymbol{\xi}_{\text{b}}$ are much smaller than the translational displacement components, Equation (9) can be obtained based on Eqs. (6) and (7).

$$\mathrm{K}_{\text{Beam}}\left(\boldsymbol{\xi}_{\text{b}},t_{\text{b}},\delta_{\text{b}}\right)=\mathbf{k}_{\text{Beam-L}}\boldsymbol{\xi}_{\text{b}}+\mathrm{K}_{\text{Beam-NL}}\left(\boldsymbol{\xi}_{\text{b}},t_{\text{b}},\delta_{\text{b}}\right)=\begin{bmatrix}12/t_{\text{b}}^2 & 0 & 0 & 0 & 0 & 0\\ 0 & 12 & 0 & 0 & 0 & -6\\ 0 & 0 & 12 & 0 & 6 & 0\\ 0 & 0 & 0 & \delta_{\text{b}} & 0 & 0\\ 0 & 0 & 6 & 0 & 4 & 0\\ 0 & -6 & 0 & 0 & 0 & 4\end{bmatrix}\boldsymbol{\xi}_{\text{b}}+\begin{bmatrix}\sigma_{\text{k-b1}}\\ \sigma_{\text{k-b2}}\\ \sigma_{\text{k-b3}}\\ \sigma_{\text{k-b4}}\\ \sigma_{\text{k-b5}}\\ \sigma_{\text{k-b6}}\end{bmatrix} \tag{9a}$$

$$\sigma_{\text{k-b1}}=\frac{36\left(35t^2-\xi_{\text{b-tx}}\right)\left(\xi_{\text{b-ty}}^2+\xi_{\text{b-tz}}^2\right)}{t^2\left(175t^2+3\xi_{\text{b-ty}}^2+3\xi_{\text{b-tz}}^2\right)},\ \sigma_{\text{k-b2}}=\frac{504\xi_{\text{b-ty}}\left(5\xi_{\text{b-tx}}+3\left(\xi_{\text{b-ty}}^2+\xi_{\text{b-tz}}^2\right)\right)}{175t^2+3\xi_{\text{b-ty}}^2+3\xi_{\text{b-tz}}^2},\ \sigma_{\text{k-b3}}=\frac{504\xi_{\text{b-tz}}\left(5\xi_{\text{b-tx}}+3\left(\xi_{\text{b-ty}}^2+\xi_{\text{b-tz}}^2\right)\right)}{175t^2+3\xi_{\text{b-ty}}^2+3\xi_{\text{b-tz}}^2},$$

$$\sigma_{\text{k-b4}}=-\frac{6\left(\xi_{\text{b-ry}}\xi_{\text{b-ty}}+\xi_{\text{b-rz}}\xi_{\text{b-tz}}\right)\left(175t^2+24\xi_{\text{b-ty}}^2+24\xi_{\text{b-tz}}^2+35\xi_{\text{b-tx}}\right)}{175t^2+3\xi_{\text{b-ty}}^2+3\xi_{\text{b-tz}}^2},\ \sigma_{\text{k-b5}}=\frac{42\xi_{\text{b-tz}}\left(5\xi_{\text{b-tx}}+3\left(\xi_{\text{b-ty}}^2+\xi_{\text{b-tz}}^2\right)\right)}{175t^2+3\xi_{\text{b-ty}}^2+3\xi_{\text{b-tz}}^2}, \tag{9b}$$

$$\sigma_{\text{k-b6}}=-\frac{42\xi_{\text{b-ty}}\left(5\xi_{\text{b-tx}}+3\left(\xi_{\text{b-ty}}^2+\xi_{\text{b-tz}}^2\right)\right)}{175t^2+3\xi_{\text{b-ty}}^2+3\xi_{\text{b-tz}}^2}$$

where $\mathbf{k}_{\text{Beam-L}}$ is the linear stiffness matrix of the wire beam, and $\mathrm{K}_{\text{Beam-NL}}(\cdot)$ is a nonlinear stiffness variable vector about the t_{b}, δ_{b} and the entries of the displacement vector $\boldsymbol{\xi}_{\text{b}}$.

In this section, the variable constraint force of a wire beam is obtained. In a similar way, the variable constraint forces produced by other basic compliant modules can also be derived based on their force-displacement relationships.

4 CFB Modelling Approach

According to Eq. (1), any force can also be written as a wrench, which can also be represented as the combination of the principal wrenches in the coordinate system. Therefore, a constant constraint force can be written as

$$\boldsymbol{F}_{cc}=\left[\, f_{cc-tx},\ f_{cc-ty},\ f_{cc-tz},\ f_{cc-rx},\ f_{cc-ry},\ f_{cc-rz} \,\right]^{T} \tag{10}$$

where $\boldsymbol{F}_{cc}$ is a wrench of a constant constraint force, while $f_{cc\text{-}tx}$, $f_{cc\text{-}ty}$, $f_{cc\text{-}tz}$, $f_{cc\text{-}rx}$, $f_{cc\text{-}ry}$, and $f_{cc\text{-}rz}$ are the components of $\boldsymbol{F}_{cc}$ along and about the three axes of the coordinate system. Different from variable constraint forces, each of the six components of a constant constraint force always has only one specified direction.

If a rigid body is balanced under the influence of n compliant modules and m external forces, the constraint force equilibrium equation for the rigid stage can be written as

$$\sum_{i=1}^{n}\left(\mathbf{T}_{vc\text{-}i}\boldsymbol{\zeta}_{vc\text{-}i}\right)+\sum_{j=1}^{m}\left(\mathbf{T}_{cc\text{-}j}\boldsymbol{F}_{cc\text{-}j}\right)=\mathbf{0} \tag{11}$$

where wrenches $\boldsymbol{\zeta}_{vc\text{-}i}$ (i=1, 2, 3 … n) and wrenches $\boldsymbol{F}_{cc\text{-}j}$ (j=1, 2, 3 … m) are the variable constraint forces of the n compliant modules and m constant constraint forces applied on this rigid stage, respectively. $\mathbf{T}_{vc\text{-}i}$ (i=1, 2, 3 … n) and $\mathbf{T}_{cc\text{-}j}$ (j=1, 2, 3 … m) are transformation matrices, which can transform all the constraint forces to any one of the coordinate systems. Based on [34], if a wrench in a coordinate system 'A' is represented as $\boldsymbol{\zeta}_a$, the wrench can be described as $\mathbf{T}_a\boldsymbol{\zeta}_a$ in a coordinate system 'B'. Here $\mathbf{T}_a$, as written in Eq. (12), is the transformation matrix from the coordinate system 'A' to the coordinate system 'B'.

$$\mathbf{T}_a=\begin{bmatrix}\mathbf{R}_{xyz} & \mathbf{0}\\ \mathbf{D}\mathbf{R}_{xyz} & \mathbf{R}_{xyz}\end{bmatrix}\ \text{where}\ \mathbf{D}=\begin{bmatrix}0 & -d_z & d_y\\ d_z & 0 & -d_x\\ -d_y & d_x & 0\end{bmatrix} \tag{12}$$

where the sub-matrix $\mathbf{R}_{xyz}$ is a 3×3 rotation matrix, and the sub-matrix $\mathbf{D}$ is a 3×3 location skew-symmetric matrix. The entries d_x, d_y and d_z in the sub-matrix $\mathbf{D}$ are the coordinates of the origin of the coordinate system 'A' in the coordinate system 'B'.

A compliant mechanism can be decomposed into rigid stages and basic compliant modules. When a compliant mechanism is at static equilibrium under the influence of a series of external forces (or constant constraint forces), all the rigid stages of the compliant mechanism are also at static equilibrium under the influence of the constant constraint forces applied and the variable constraint forces of the basic compliant modules. As studied in Section 3, the variable constraint forces of the basic compliant modules can be derived based on the force-displacement relationships of the basic compliant modules. Therefore, the constraint force equilibrium equations for all the rigid stages can be represented by the variable constraint forces and the constant constraint forces. Moreover, the analytical model of the compliant mechanism can be calculated based on the constraint force equilibrium equations.

If a compliant mechanism is decomposed into rigid stages and non-basic compliant modules, the non-basic compliant modules can be regarded as sub-compliant mechanisms. The sub-compliant mechanisms can be analytically modelled based on the approach detailed above, and then the variable constraint forces of the sub-compliant mechanisms can be derived from the analytical model. Therefore, the compliant modules, in the CFB modelling approach, can be basic compliant modules and non-basic compliant modules. In practical use, the CFB modelling approach usually decomposes a complex compliant mechanism into non-basic compliant modules, and the variable constraint force of each of the non-basic compliant modules is derived via further decomposing the non-basic compliant module into basic compliant modules.

Note that if all the nonlinear contributions in the variable constraint forces are not considered and the transformation matrices are derived based on the undeformed configuration of a compliant mechanism, the linear analytical model of the compliant mechanism can be obtained; otherwise, the nonlinear analytical model of the compliant mechanism can be derived.

5 Case Studies

In this section, an XYZ CPM, as shown in Fig. 1(a), is modelled using the CFB modelling approach. It can be seen from Fig. 1(c) that the XYZ CPM can be decomposed into PMs and AMs. Each of the PMs is a four-beam non-basic compliant module, and each of the AMs is an eight-beam non-basic compliant module. The variable constraint forces of the four-beam and eight-beam non-basic compliant modules are derived in Sections 5.1 and 5.2, and then the XYZ CPM is modelled based on the derived variable constraint forces in Section 5.3.

5.1 Variable Constraint Force of the Four-Beam Non-Basic Compliant Module

One of the four-beam non-basic compliant modules (or the PMs as shown in Fig. 1(c)) is shown in Fig. 4. Suppose that the thickness of the mobile top plate is tiny compared with the length of the beams. Four wrenches, $\boldsymbol{\zeta}_{fbi}$ (i=1, 2, 3 and 4), are used to represent the variable constraint forces of the four beams in the local coordinate systems O_{fbi}-$X_{fbi}Y_{fbi}Z_{fbi}$ (i=1, 2, 3 and 4), respectively. Note that the local coordinate systems are placed at the tips of the four beams, O_{fb1}, O_{fb2}, O_{fb3} and O_{fb4} shown in Fig. 4, respectively. If the displacement of the four-beam non-basic compliant module is $\boldsymbol{\xi}_{fb}$ in the global coordinate system, the displacements, $\boldsymbol{\xi}_{fbi}$, of the tips of the four beams can be written as

$$\boldsymbol{\xi}_{fbi}=\left[\mathbf{T}_{fbi\text{-}fb}\right]^{T}\boldsymbol{\xi}_{fb}\quad i=1,2,3\,\text{and}\,4,\,\text{respectively} \tag{13}$$

where $\mathbf{T}_{fbi\text{-}fb}$ (i=1, 2, 3 and 4) are the transformation matrices from the local coordinate systems O_{fbi}-$X_{fbi}Y_{fbi}Z_{fbi}$ to the global coordinate system O_{fb}-$X_{fb}Y_{fb}Z_{fb}$, respectively. When the rotational displacements of the top plate are tiny compared with the translational displacements, the transformation matrices can be obtained as shown in Eq. (14) based on Eq. (12).

$$\mathbf{T}_{\mathrm{fb}i\text{-}\mathrm{fb}}=\begin{bmatrix}1&0&0&0&0&0\\0&1&0&0&0&0\\0&0&1&0&0&0\\0&\sigma_{\mathrm{fb}i-1}&\sigma_{\mathrm{fb}i-2}&1&0&0\\\sigma_{\mathrm{fb}i-3}&0&0&0&1&0\\\sigma_{\mathrm{fb}i-4}&0&0&0&0&1\end{bmatrix} \tag{14a}$$

$$\sigma_{\mathrm{fb}1-1}=\sigma_{\mathrm{fb}1-4}=\sigma_{\mathrm{fb}2-1}=\sigma_{\mathrm{fb}2-2}=\sigma_{\mathrm{fb}3-2}=\sigma_{\mathrm{fb}3-3}=\sigma_{\mathrm{fb}4-3}=\sigma_{\mathrm{fb}4-4}=\left(t_{\mathrm{fb}}-w_{\mathrm{fb}}\right)/2 \tag{14b}$$

$$\sigma_{\mathrm{fb}1-2}=\sigma_{\mathrm{fb}1-3}=\sigma_{\mathrm{fb}2-3}=\sigma_{\mathrm{fb}2-4}=\sigma_{\mathrm{fb}3-1}=\sigma_{\mathrm{fb}3-4}=\sigma_{\mathrm{fb}4-1}=\sigma_{\mathrm{fb}4-2}=\left(w_{\mathrm{fb}}-t_{\mathrm{fb}}\right)/2 \tag{14c}$$

where w_{fb} is the width of the square mobile plate of the four-beam non-basic compliant module. t_{fb} is the thickness of the beam (in this example, all beams have the same thickness, i.e. $t_{\mathrm{fb}1}= t_{\mathrm{fb}2}= t_{\mathrm{fb}3}= t_{\mathrm{fb}4}=t_{\mathrm{fb}}$). Based on Eq. (8), the variable constraint forces produced by the four beams can be obtained, as shown in Eq. (15). The variable constraint force, $\boldsymbol{\zeta}_{\mathrm{fb}}$, of the four-beam non-basic compliant module is the vector sum of the variable constraint forces of the four beams, which can be written as Eq. (16) according to Eq. (11).

$$\boldsymbol{\zeta}_{\mathrm{fb}i}=-\mathrm{K}_{\mathrm{Beam}}\left(\boldsymbol{\xi}_{\mathrm{fb}i},t_{\mathrm{fb}i},\delta_{\mathrm{fb}i}\right)\ i=1,2,3\text{and}\,4,\text{respectively} \tag{15}$$

$$\boldsymbol{\zeta}_{\mathrm{fb}}=\sum_{i=1}^{4}\left(\mathbf{T}_{\mathrm{fb}i\text{-}\mathrm{fb}}\boldsymbol{\zeta}_{\mathrm{fb}i}\right) \tag{16}$$

Combining Eqs. (9) and (13) – (16), the variable constraint force of the four-beam non-basic compliant module can be derived. Suppose that the rotational displacements of the four-beam non-basic compliant module about the X_{fd}-, Y_{fd}- and Z_{fd}-axes are much smaller than the translational displacements along the X_{fd}-, Y_{fd}- and Z_{fd}-axes, the components, $\zeta_{\mathrm{fb}\text{-}tx}$, $\zeta_{\mathrm{fb}\text{-}ty}$, $\zeta_{\mathrm{fb}\text{-}tz}$, $\zeta_{\mathrm{fb}\text{-}rx}$, $\zeta_{\mathrm{fb}\text{-}ry}$ and $\zeta_{\mathrm{fb}\text{-}rz}$, of the wrench $\boldsymbol{\zeta}_{\mathrm{fb}}$ can be simplified, as shown in Eq. (17). For convenience, Eq. (17) can also be rewritten as Eq. (18). If $\boldsymbol{F}_{\mathrm{fb}}$ is a force to balance the variable constraint force $\boldsymbol{\zeta}_{\mathrm{fb}}$, $\boldsymbol{F}_{\mathrm{fb}}$ can be written as Eq. (19), which is the force-displacement relationship of the four-beam non-basic compliant module.

$$\zeta_{\mathrm{fb}\text{-}tx}=-\frac{1680\left(5\xi_{\mathrm{fb}\text{-}tx}+3\left(\xi_{\mathrm{fb}\text{-}ty}^2+\xi_{\mathrm{fb}\text{-}tz}^2\right)\right)}{175t_{\mathrm{fb}}^2+3\xi_{\mathrm{fb}\text{-}ty}^2+3\xi_{\mathrm{fb}\text{-}tz}^2} \tag{17a}$$

$$\zeta_{\mathrm{fb}\text{-}ty}=-\frac{48\xi_{\mathrm{fb}\text{-}ty}\left(175t_{\mathrm{fb}}^2+210\xi_{\mathrm{fb}\text{-}tx}+129\xi_{\mathrm{fb}\text{-}ty}^2+129\xi_{\mathrm{fb}\text{-}tz}^2\right)}{175t_{\mathrm{fb}}^2+3\xi_{\mathrm{fb}\text{-}ty}^2+3\xi_{\mathrm{fb}\text{-}tz}^2} \tag{17b}$$

$$\zeta_{\mathrm{fb}\text{-}tz}=-\frac{48\xi_{\mathrm{fb}\text{-}tz}\left(175t_{\mathrm{fb}}^2+210\xi_{\mathrm{fb}\text{-}tx}+129\xi_{\mathrm{fb}\text{-}ty}^2+129\xi_{\mathrm{fb}\text{-}tz}^2\right)}{175t_{\mathrm{fb}}^2+3\xi_{\mathrm{fb}\text{-}ty}^2+3\xi_{\mathrm{fb}\text{-}tz}^2} \tag{17c}$$

$$\zeta_{\mathrm{fb}\text{-}rx}=-\frac{4\left(\delta_{\mathrm{fb}}\xi_{\mathrm{fb}\text{-}rx}\left(3\xi_{\mathrm{fb}\text{-}ty}^2+3\xi_{\mathrm{fb}\text{-}tz}^2+175t_{\mathrm{fb}}^2\right)-210\left(5t_{\mathrm{fb}}^2-3t_{\mathrm{fb}}w_{\mathrm{fb}}+3w_{\mathrm{fb}}^2\right)\left(\xi_{\mathrm{fb}\text{-}ry}\xi_{\mathrm{fb}\text{-}ty}+\xi_{\mathrm{fb}\text{-}rz}\xi_{\mathrm{fb}\text{-}tz}\right)\right)}{3\xi_{\mathrm{fb}\text{-}ty}^2+3\xi_{\mathrm{fb}\text{-}tz}^2+175t_{\mathrm{fb}}^2} \tag{17d}$$

$$\zeta_{\mathrm{fb}\text{-}ry}=-\frac{4\left(175\left(4t_{\mathrm{fb}}^2-3t_{\mathrm{fb}}w_{\mathrm{fb}}+3w_{\mathrm{fb}}^2\right)\xi_{\mathrm{fb}\text{-}ry}+6\xi_{\mathrm{fb}\text{-}tz}\left(35\xi_{\mathrm{fb}\text{-}tx}+24\xi_{\mathrm{fb}\text{-}ty}^2+24\xi_{\mathrm{fb}\text{-}tz}^2+175t_{\mathrm{fb}}^2\right)\right)}{3\xi_{\mathrm{fb}\text{-}ty}^2+3\xi_{\mathrm{fb}\text{-}tz}^2+175t_{\mathrm{fb}}^2} \tag{17e}$$

$$\zeta_{\mathrm{fb}\text{-}rz}=-\frac{4\left(175\left(4t_{\mathrm{fb}}^2-3t_{\mathrm{fb}}w_{\mathrm{fb}}+3w_{\mathrm{fb}}^2\right)\xi_{\mathrm{fb}\text{-}rz}-6\xi_{\mathrm{fb}\text{-}ty}\left(35\xi_{\mathrm{fb}\text{-}tx}+24\xi_{\mathrm{fb}\text{-}ty}^2+24\xi_{\mathrm{fb}\text{-}tz}^2+175t_{\mathrm{fb}}^2\right)\right)}{3\xi_{\mathrm{fb}\text{-}ty}^2+3\xi_{\mathrm{fb}\text{-}tz}^2+175t_{\mathrm{fb}}^2} \tag{17f}$$

$$\boldsymbol{\zeta}_{\mathrm{fb}}=-\mathrm{K}_{\mathrm{FBeam}}\left(\boldsymbol{\xi}_{\mathrm{fb}},w_{\mathrm{fb}},t_{\mathrm{fb}},\delta_{\mathrm{fb}}\right)=-\left[\zeta_{\mathrm{fb}\text{-}tx},\zeta_{\mathrm{fb}\text{-}ty},\zeta_{\mathrm{fb}\text{-}tz},\zeta_{\mathrm{fb}\text{-}rx},\zeta_{\mathrm{fb}\text{-}ry},\zeta_{\mathrm{fb}\text{-}rz}\right]^{\mathrm{T}} \tag{18}$$

$$\boldsymbol{F}_{\mathrm{fb}}=\mathrm{K}_{\mathrm{FBeam}}\left(\boldsymbol{\xi}_{\mathrm{fb}},w_{\mathrm{fb}},t_{\mathrm{fb}},\delta_{\mathrm{fb}}\right) \tag{19}$$

where $\delta_{\mathrm{fb}}=1/(1+\upsilon_{\mathrm{fb}})$, here υ_{fb} is the Poisson's ratio of the material (in this example, all beams are made of the same material, i.e. $\delta_{\mathrm{fb}1}=\delta_{\mathrm{fb}2}= \delta_{\mathrm{fb}3}=\delta_{\mathrm{fb}4}=\delta_{\mathrm{fb}}$). When only linear part in Eq. (9) is considered (i.e. $\mathrm{K}_{\mathrm{Beam}}(\boldsymbol{\xi}_{\mathrm{b}}, t_{\mathrm{b}}, \delta_{\mathrm{b}})=\mathbf{k}_{\mathrm{Beam\text{-}L}}\boldsymbol{\xi}_{\mathrm{b}}$), $\boldsymbol{\zeta}_{\mathrm{fb}}$ can be simplified as

$$\boldsymbol{\zeta}_{\mathrm{fb}}=-\mathrm{K}_{\mathrm{FBeam}}\left(\boldsymbol{\xi}_{\mathrm{fb}},w_{\mathrm{fb}},t_{\mathrm{fb}},\delta_{\mathrm{fb}}\right)=-\mathbf{k}_{\mathrm{FBeam\text{-}L}}\boldsymbol{\xi}_{\mathrm{fb}}=-\begin{bmatrix}\sigma_{\mathrm{k}\text{-}\mathrm{fb}1}&0&0&0&0&0\\0&48&0&0&0&-24\\0&0&48&0&24&0\\0&0&0&\sigma_{\mathrm{k}\text{-}\mathrm{fb}2}&0&0\\0&0&24&0&\sigma_{\mathrm{k}\text{-}\mathrm{fb}3}&0\\0&-24&0&0&0&\sigma_{\mathrm{k}\text{-}\mathrm{fb}3}\end{bmatrix}\boldsymbol{\xi}_{\mathrm{fb}} \tag{20a}$$

$$\begin{aligned}\sigma_{\mathrm{k}\text{-}\mathrm{fb}1}&=48/t_{\mathrm{fb}}^2\\\sigma_{\mathrm{k}\text{-}\mathrm{fb}2}&=4\left(6t_{\mathrm{fb}}^2-12w_{\mathrm{fb}}t_{\mathrm{fb}}+6w_{\mathrm{fb}}^2+\delta_{\mathrm{fb}}\right)\\\sigma_{\mathrm{k}\text{-}\mathrm{fb}3}&=4\left(7t_{\mathrm{fb}}^2-6w_{\mathrm{fb}}t_{\mathrm{fb}}+3w_{\mathrm{fb}}^2\right)/t_{\mathrm{fb}}^2\end{aligned} \tag{20b}$$

where $\mathbf{k}_{\mathrm{FBeam\text{-}L}}$ is the linear stiffness matrix of the four-beam non-basic compliant module.

5.2 Variable Constraint Force of the Eight-Beam Non-Basic Compliant Module

Each of the eight-beam non-basic compliant modules (or the AMs shown in Fig. 1(c)) can be decomposed into one mobile rigid stage (MRS) and two four-beam non-basic compliant modules (termed as CM-1 and CM-2), as shown in Fig. 5(a). The CM-1 and the CM-2 have the same dimension. In this example, the eight-beam non-basic compliant module is decomposed into two four-beam non-basic compliant modules, because the variable constraint force of the four-beam non-basic compliant module has been obtained in Section 5.1.

A coordinate system O_{eb}-$X_{eb}Y_{eb}Z_{eb}$ is defined as the global coordinate system, which is located at the center of the MRS. Coordinate systems O_{eb1}-$X_{eb1}Y_{eb1}Z_{eb1}$, O_{eb2}-$X_{eb2}Y_{eb2}Z_{eb2}$ and O_{ebf}-$X_{ebf}Y_{ebf}Z_{ebf}$ are defined as the local coordinate systems. The global and local coordinate systems can be seen in Fig. 5(b). The origin of the coordinate system, O_{eb}-$X_{eb}Y_{eb}Z_{eb}$, is at the center of the MRS, and the coordinate systems, O_{eb1}-$X_{eb1}Y_{eb1}Z_{eb1}$, O_{eb2}-$X_{eb2}Y_{eb2}Z_{eb2}$ and O_{ebf}-$X_{ebf}Y_{ebf}Z_{ebf}$, are placed at the centers of the three surfaces of the MRS, respectively. Note that the global coordinate system is fixed to the BSs, and the local coordinate systems are fixed to the MRS.

The displacement vector, $\boldsymbol{\xi}_{eb}$, of the MRS in the global coordinate system is written in Eq. (21), and the displacement vectors of the CM-1 and CM-2 are represented as $\boldsymbol{\xi}_{ef1}$ in the local coordinate system O_{eb1}-$X_{eb1}Y_{eb1}Z_{eb1}$ and $\boldsymbol{\xi}_{ef2}$ in the local coordinate system O_{eb2}-$X_{eb2}Y_{eb2}Z_{eb2}$, respectively. The displacement vectors $\boldsymbol{\xi}_{ef1}$ and $\boldsymbol{\xi}_{ef1}$ are shown in Eq. (22).

$$\boldsymbol{\xi}_{eb}=\left[\xi_{eb\text{-}tx},\xi_{eb\text{-}ty},\xi_{eb\text{-}tz},\xi_{eb\text{-}rx},\xi_{eb\text{-}ry},\xi_{eb\text{-}rz}\right]^{\mathrm{T}} \tag{21}$$

$$\boldsymbol{\xi}_{eb1}=\left[\mathbf{T}_{eb1\text{-}eb}\right]^{\mathrm{T}}\boldsymbol{\xi}_{eb} \text{ and } \boldsymbol{\xi}_{eb2}=\left[\mathbf{T}_{eb2\text{-}eb}\right]^{\mathrm{T}}\boldsymbol{\xi}_{eb} \tag{22}$$

where $\xi_{eb\text{-}tx}$, $\xi_{eb\text{-}ty}$, $\xi_{eb\text{-}tz}$, $\xi_{eb\text{-}rx}$, $\xi_{eb\text{-}ry}$ and $\xi_{eb\text{-}rz}$ are the displacements of the MRS along and about the X_{eb}-, Y_{eb}- and Z_{eb}-axes of the global coordinate system. $\mathbf{T}_{eb1\text{-}eb}$ and $\mathbf{T}_{eb2\text{-}eb}$, obtained based on Eq. (12) and shown in Eq. (23), are the transformation matrices from the local coordinate systems O_{eb1}-$X_{eb1}Y_{eb1}Z_{eb1}$ and O_{eb2}-$X_{eb2}Y_{eb2}Z_{eb2}$ to the global coordinate system O_{eb}-$X_{eb}Y_{eb}Z_{eb}$, respectively. The transformation matrix from the local coordinate system O_{ebf}-$X_{ebf}Y_{ebf}Z_{ebf}$ to the global coordinate system is $\mathbf{T}_{ebf\text{-}eb}$, which is also illustrated in Eq. (23). Note that the effect of the MRS's rotations on the transformation matrices is ignored, because the rotational displacements are much smaller than the translational displacements of the MRS.

$$\mathbf{T}_{eb1\text{-}eb}=\begin{bmatrix}0&0&-1&0&0&0\\0&1&0&0&0&0\\1&0&0&0&0&0\\0&\dfrac{w_{eb}}{2}&0&0&0&-1\\0&0&\dfrac{w_{eb}}{2}&0&1&0\\0&0&0&1&0&0\end{bmatrix},\ \mathbf{T}_{eb2\text{-}eb}=\begin{bmatrix}0&0&1&0&0&0\\1&0&0&0&0&0\\0&1&0&0&0&0\\0&-\dfrac{w_{eb}}{2}&0&0&0&1\\0&0&0&1&0&0\\0&0&\dfrac{w_{eb}}{2}&0&1&0\end{bmatrix} \text{ and } \mathbf{T}_{ebf\text{-}eb}=\begin{bmatrix}1&0&0&0&0&0\\0&1&0&0&0&0\\0&0&1&0&0&0\\0&0&0&1&0&0\\0&0&\dfrac{w_{eb}}{2}&0&1&0\\0&-\dfrac{w_{eb}}{2}&0&0&0&1\end{bmatrix} \tag{23}$$

where w_{eb} is the edge length of the MRS. Based on Eq. (18), the variable constraint force offered by the CM-1 and CM-2 can be obtained, as shown in Eq. (24).

$$\zeta_{eb1}=-\mathrm{K}_{\mathrm{FBeam}}\left(\xi_{eb1},w_{eb1},t_{eb1},\delta_{eb1}\right) \text{ and } \zeta_{eb2}=-\mathrm{K}_{\mathrm{FBeam}}\left(\xi_{eb2},w_{eb2},t_{eb2},\delta_{eb2}\right) \tag{24}$$

In this example, the CM-1 and CM-2 have the same dimension and material, so $w_{eb1}=w_{eb2}=w_{eb}$, $t_{eb1}=t_{eb2}=t_{eb}$ and $\delta_{eb1}=\delta_{eb2}=\delta_{eb}$. Furthermore, Equation (25) can be derived on the basis of Eq. (11).

$$\boldsymbol{\zeta}_{eb}=\mathbf{T}_{eb1\text{-}eb}\boldsymbol{\zeta}_{eb1}+\mathbf{T}_{eb2\text{-}eb}\boldsymbol{\zeta}_{eb2} \tag{25}$$

Combining Eqs. (17), (18) and (22) – (25), the variable constraint force, $\boldsymbol{\zeta}_{eb}$, of the eight-beam non-basic compliant module can be obtained. Because the rotational displacements of the MRS are tiny compared with the translational displacements, the $\boldsymbol{\zeta}_{eb}$ can be simplified as shown in Eq. (26), which can also be rewritten as shown in Eq. (27). If a force $\boldsymbol{F}_{eb}$ is applied on the eight-beam parallel compliant module in the local coordinate system O_{ebf}-$X_{ebf}Y_{ebf}Z_{ebf}$, to balance the $\boldsymbol{\zeta}_{eb}$, the force-displacement relationship of the eight-beam non-basic compliant module can be represented as shown in Eq. (28).

$$\zeta_{eb\text{-}tx}=-\frac{96\xi_{eb\text{-}tx}\left(129\xi_{eb\text{-}tx}^2+35\left(5t_{eb}^2+3\xi_{eb\text{-}ty}+3\xi_{eb\text{-}tz}\right)\right)}{175t_{eb}^2+3\xi_{eb\text{-}tx}^2} \tag{26a}$$

$$\zeta_{eb\text{-}ty}=-\frac{24\left(6\left(43\xi_{eb\text{-}ty}+35\right)\xi_{eb\text{-}tx}^2+70\xi_{eb\text{-}ty}\left(5t_{eb}^2+6\xi_{eb\text{-}tz}+5\right)+w_{eb}\xi_{eb\text{-}rx}\left(129\xi_{eb\text{-}tx}^2+35\left(5t_{eb}^2+6\xi_{eb\text{-}tz}\right)\right)\right)}{175t_{eb}^2+3\xi_{eb\text{-}tx}^2} \tag{26b}$$

$$\zeta_{eb\text{-}tz}=\frac{24\left(w_{eb}\xi_{eb\text{-}rx}\left(129\xi_{eb\text{-}tx}^2+35\left(5t_{eb}^2+6\xi_{eb\text{-}ty}\right)\right)-2\left(3\left(43\xi_{eb\text{-}tz}+35\right)\xi_{eb\text{-}tx}^2+35\left(5t_{eb}^2+6\xi_{eb\text{-}ty}+5\right)\xi_{eb\text{-}tz}\right)\right)}{175t_{eb}^2+3\xi_{eb\text{-}tx}^2} \tag{26c}$$

$$\zeta_{eb\text{-}rx}=-\frac{4}{175t_{eb}^2+3\xi_{eb\text{-}tx}^2}\begin{pmatrix}6\left(175\left(w_{eb}+1\right)t_{eb}^2+3\left(43w_{eb}+8\right)\xi_{eb\text{-}tx}^2\right)\left(\xi_{eb\text{-}ty}-\xi_{eb\text{-}tz}\right)\\+\xi_{eb\text{-}rx}\left(18w_{eb}\left(43w_{eb}+8\right)\xi_{eb\text{-}tx}^2+35\left(10\left(\left(3w_{eb}^2+3w_{eb}+4\right)t_{eb}^2-3w_{eb}t_{eb}+3w_{eb}^2\right)+3w_{eb}\left(6w_{eb}+1\right)\xi_{eb\text{-}ty}+3w_{eb}\left(6w_{eb}+1\right)\xi_{eb\text{-}tz}\right)\right)\end{pmatrix} \tag{26d}$$

$$\zeta_{\text{eb-ry}}=-\frac{-4}{175t_{\text{eb}}^2+3\xi_{\text{eb-tx}}^2}\begin{pmatrix}6\xi_{\text{eb-tx}}\left(3\left(43w_{\text{eb}}+8\right)\xi_{\text{eb-tx}}^2+35\left(5t_{\text{eb}}^2-3w_{\text{eb}}t_{\text{eb}}+3w_{\text{eb}}^2\right)\xi_{\text{eb-rx}}+35\left(5\left(w_{\text{eb}}+1\right)t_{\text{eb}}^2+\left(6w_{\text{eb}}+1\right)\xi_{\text{eb-tz}}\right)\right)\\-\xi_{\text{eb-ry}}\left(3\delta\xi_{\text{eb-tx}}^2+175\left(\left(\delta_{\text{eb}}+4\right)t_{\text{eb}}^2-3w_{\text{eb}}t_{\text{eb}}+3w_{\text{eb}}^2\right)\right)\end{pmatrix} \tag{26e}$$

$$\zeta_{\text{eb-rz}}=-\frac{4}{175t_{\text{eb}}^2+3\xi_{\text{eb-tx}}^2}\begin{pmatrix}\xi_{\text{eb-rz}}\left(3\delta_{\text{eb}}\xi_{\text{eb-tx}}^2+175\left(\left(\delta_{\text{eb}}+4\right)t_{\text{eb}}^2-3w_{\text{eb}}t_{\text{eb}}+3w_{\text{eb}}^2\right)\right)\\+6\xi_{\text{eb-tx}}\left(3\left(43w_{\text{eb}}+8\right)\xi_{\text{eb-tx}}^2-35\left(5t_{\text{eb}}^2-3w_{\text{eb}}t_{\text{eb}}+3w_{\text{eb}}^2\right)\xi_{\text{eb-rx}}+35\left(5\left(w_{\text{eb}}+1\right)t_{\text{eb}}^2+\left(6w_{\text{eb}}+1\right)\xi_{\text{eb-ty}}\right)\right)\end{pmatrix} \tag{26f}$$

$$\boldsymbol{\zeta}_{\text{eb}}=-\mathrm{K}_{\text{EBeam}}\left(\boldsymbol{\xi}_{\text{eb}},w_{\text{eb}},t_{\text{eb}},\delta_{\text{eb}}\right)=-\left[\zeta_{\text{eb-tx}},\zeta_{\text{eb-ty}},\zeta_{\text{eb-tz}},\zeta_{\text{eb-rx}},\zeta_{\text{eb-ry}},\zeta_{\text{eb-rz}}\right]^{\mathrm{T}} \tag{27}$$

$$\boldsymbol{F}_{\text{eb}}=\left[\mathbf{T}_{\text{ebf-eb}}\right]^{-1}\mathrm{K}_{\text{EBeam}}\left(\boldsymbol{\xi}_{\text{eb}},w_{\text{eb}},t_{\text{eb}},\delta_{\text{eb}}\right) \tag{28}$$

When only linear part of the variable constraint force of the four-beam non-basic compliant module is considered (i.e. $\mathrm{K}_{\text{FBeam}}(\boldsymbol{\xi}_{\text{b}}, t_{\text{b}}, \delta_{\text{b}})=\mathbf{k}_{\text{FBeam-L}}\boldsymbol{\xi}_{\text{Fb}}$ as shown in Eq. (20)), $\boldsymbol{\zeta}_{\text{eb}}$ can be simplified as shown in Eq. (29).

$$\boldsymbol{\zeta}_{\text{eb}}=-\mathrm{K}_{\text{EBeam}}\left(\boldsymbol{\xi}_{\text{eb}},w_{\text{eb}},t_{\text{eb}},\delta_{\text{eb}}\right)=-\mathbf{k}_{\text{EBeam-L}}\boldsymbol{\xi}_{\text{eb}}=-\begin{bmatrix}96&0&0&0&-\sigma_{\text{k-eb2}}&\sigma_{\text{k-eb2}}\\0&\sigma_{\text{k-eb1}}&0&\sigma_{\text{k-eb2}}&0&0\\0&0&\sigma_{\text{k-eb1}}&-\sigma_{\text{k-eb2}}&0&0\\0&\sigma_{\text{k-eb2}}&-\sigma_{\text{k-eb2}}&\sigma_{\text{k-eb3}}&0&0\\-\sigma_{\text{k-eb2}}&0&0&0&\sigma_{\text{k-eb4}}&0\\\sigma_{\text{k-eb2}}&0&0&0&0&\sigma_{\text{k-eb4}}\end{bmatrix}\boldsymbol{\xi}_{\text{eb}} \tag{29a}$$

$$\begin{aligned}\sigma_{\text{k-eb1}}&=48\left(1+1/t_{\text{eb}}^2\right)\\\sigma_{\text{k-eb2}}&=24\left(w_{\text{eb}}+1\right)\\\sigma_{\text{k-eb3}}&=8\left(\left(3w_{\text{eb}}^2+6w_{\text{eb}}+7\right)t_{\text{eb}}^2-6w_{\text{eb}}t_{\text{eb}}+3w_{\text{eb}}^2\right)/t_{\text{eb}}^2\\\sigma_{\text{k-eb4}}&=4\left(6t_{\text{eb}}^4-12wt_{\text{eb}}^3+\left(9w_{\text{eb}}^2+6w_{\text{eb}}+\delta_{\text{eb}}+7\right)t_{\text{eb}}^2-6w_{\text{eb}}t_{\text{eb}}+3w_{\text{eb}}^2\right)/t_{\text{eb}}^2\end{aligned} \tag{29b}$$

where $\mathbf{k}_{\text{EBeam-L}}$ is the linear stiffness matrix of the eight-beam non-basic compliant module.

5.3 Modelling of an XYZ CPM

The XYZ CPM (as shown in Fig. 1(a)) is modelled using the CFB modelling approach in this section, based on the variable constraint forces of the four-beam and eight-beam non-basic compliant modules (PMs and AMs) derived in Sections 5.1 and 5.2. As shown in Fig. 1(c), the MRSs (mobile rigid stages) of the eight-beam non-basic compliant modules are also the actuated stages (ASs) of the XYZ CPM.

The defined coordinate systems are demonstrated in Fig. 6. The global coordinate system $\mathrm{O_m}$-$\mathrm{X_mY_mZ_m}$ is fixed to the ground, and the other local coordinate systems are fixed to the connected rigid stages, respectively. Each of the local coordinate systems can translate with the connected rigid stage, but cannot rotate with the connected rigid stage. When the XYZ CPM is at the undeformed configuration, the positions of the local coordinate systems are defined as the original positions of the local coordinate systems. Compared with these original positions, the displacements of the origins of the local coordinate systems $\mathrm{O_{pmx}}$-$\mathrm{X_{pmx}Y_{pmx}Z_{pmx}}$, $\mathrm{O_{pmy}}$-$\mathrm{X_{pmy}Y_{pmy}Z_{pmy}}$, $\mathrm{O_{pmz}}$-$\mathrm{X_{pmz}Y_{pmz}Z_{pmz}}$, $\mathrm{O_{asx}}$-$\mathrm{X_{asx}Y_{asx}Z_{asx}}$, $\mathrm{O_{amx}}$-$\mathrm{X_{amx}Y_{amx}Z_{amx}}$, $\mathrm{O_{pax}}$-$\mathrm{X_{pax}Y_{pax}Z_{pax}}$, $\mathrm{O_{asy}}$-$\mathrm{X_{asy}Y_{asy}Z_{asy}}$, $\mathrm{O_{amy}}$-$\mathrm{X_{amy}Y_{amy}Z_{amy}}$, $\mathrm{O_{pay}}$-$\mathrm{X_{pay}Y_{pay}Z_{pay}}$, $\mathrm{O_{asz}}$-$\mathrm{X_{asz}Y_{asz}Z_{asz}}$, $\mathrm{O_{amz}}$-$\mathrm{X_{amz}Y_{amz}Z_{amz}}$, and $\mathrm{O_{paz}}$-$\mathrm{X_{paz}Y_{paz}Z_{paz}}$ are represented as displacement vectors $\boldsymbol{\xi}_{\text{pmx}}$, $\boldsymbol{\xi}_{\text{pmy}}$, $\boldsymbol{\xi}_{\text{pmz}}$, $\boldsymbol{\xi}_{\text{asx}}$, $\boldsymbol{\xi}_{\text{amx}}$, $\boldsymbol{\xi}_{\text{pax}}$, $\boldsymbol{\xi}_{\text{asy}}$, $\boldsymbol{\xi}_{\text{amy}}$, $\boldsymbol{\xi}_{\text{pay}}$, $\boldsymbol{\xi}_{\text{asz}}$, $\boldsymbol{\xi}_{\text{amz}}$, and $\boldsymbol{\xi}_{\text{paz}}$, when the XYZ CPM is at a deformed configuration. Additionally, the displacement of the top center of the MS is represented as $\boldsymbol{\xi}_{\text{m}}$ in the global coordinate system.

Based on Eq. (12), the associated transformation matrices are defined as $\mathbf{T}_{\text{pmx-m}}$, $\mathbf{T}_{\text{pmy-m}}$, $\mathbf{T}_{\text{pmz-m}}$, $\mathbf{T}_{\text{pax-pmx}}$, $\mathbf{T}_{\text{pay-pmy}}$, $\mathbf{T}_{\text{paz-pmz}}$, $\mathbf{T}_{\text{pmx-pax}}$, $\mathbf{T}_{\text{pmy-pay}}$, $\mathbf{T}_{\text{pmz-paz}}$, $\mathbf{T}_{\text{pax-asx}}$, $\mathbf{T}_{\text{pay-asy}}$, $\mathbf{T}_{\text{paz-asz}}$, $\mathbf{T}_{\text{amx-asx}}$, $\mathbf{T}_{\text{amy-asy}}$ and $\mathbf{T}_{\text{amz-asz}}$. The subscript of each of the transformation matrices shows the associated coordinate systems and the transformation between them. For instance, the subscript 'pmx-m' in $\mathbf{T}_{\text{pmx-m}}$ indicates that $\mathbf{T}_{\text{pmx-m}}$ is the transformation matrix from the coordinate system $\mathrm{O_{pmx}}$-$\mathrm{X_{pmx}Y_{pmx}Z_{pmx}}$ to the coordinate system $\mathrm{O_m}$-$\mathrm{X_mY_mZ_m}$. After deformation of the XYZ CPM, the transformation matrices can be written as Eqs. (A.1) – (A.15) in Appendix A. Note that all the tiny displacements such as the parasitic rotations in the transformation matrices are ignored.

On the basis of the conditions of geometric compatibility [17], Equation (30) can be obtained. It can be seen that $\boldsymbol{\xi}_{\text{amx}}$, $\boldsymbol{\xi}_{\text{amy}}$ and $\boldsymbol{\xi}_{\text{amz}}$ are also the deformation displacements of the AM-X, AM-Y and AM-Z, respectively. In addition, the deformation displacements of the PM-X, PM-Y and PM-Z can also be derived, which can be represented as $\boldsymbol{\xi}_{\text{pmx-pax}}$, $\boldsymbol{\xi}_{\text{pmy-pay}}$ and $\boldsymbol{\xi}_{\text{pmz-paz}}$ in the coordinate systems $\mathrm{O_{pmx}}$-$\mathrm{X_{pmx}Y_{pmx}Z_{pmx}}$, $\mathrm{O_{pmy}}$-$\mathrm{X_{pmy}Y_{pmy}Z_{pmy}}$ and $\mathrm{O_{pmz}}$-$\mathrm{X_{pmz}Y_{pmz}Z_{pmz}}$, respectively (these three coordinate systems are at their original positions). The $\boldsymbol{\xi}_{\text{pmx-pax}}$, $\boldsymbol{\xi}_{\text{pmy-pay}}$ and $\boldsymbol{\xi}_{\text{pmz-paz}}$ can be seen in Eq. (31).

$$\boldsymbol{\xi}_{\text{pmx}}=\left[\mathbf{T}_{\text{pmx-m}}\right]^{\mathrm{T}}\boldsymbol{\xi}_{\text{m}},\ \boldsymbol{\xi}_{\text{pmy}}=\left[\mathbf{T}_{\text{pmy-m}}\right]^{\mathrm{T}}\boldsymbol{\xi}_{\text{m}},\ \boldsymbol{\xi}_{\text{pmz}}=\left[\mathbf{T}_{\text{pmz-m}}\right]^{\mathrm{T}}\boldsymbol{\xi}_{\text{m}} \tag{30a}$$

$$\boldsymbol{\xi}_{\text{amx}}=\left[\mathbf{T}_{\text{amx-asx}}\right]^{\mathrm{T}}\boldsymbol{\xi}_{\text{asx}}\ \text{and}\ \boldsymbol{\xi}_{\text{pax}}=\left[\mathbf{T}_{\text{pax-asx}}\right]^{\mathrm{T}}\boldsymbol{\xi}_{\text{asx}} \tag{30b}$$

$$\boldsymbol{\xi}_{\text{amy}}=\left[\mathbf{T}_{\text{amy-asy}}\right]^{\mathrm{T}}\boldsymbol{\xi}_{\text{asy}}\ \text{and}\ \boldsymbol{\xi}_{\text{pay}}=\left[\mathbf{T}_{\text{pay-asy}}\right]^{\mathrm{T}}\boldsymbol{\xi}_{\text{asy}} \tag{30c}$$

$$\xi_{amz}=\left[\mathbf{T}_{amz\text{-}asz}\right]^{T}\xi_{asz} \text{ and } \xi_{paz}=\left[\mathbf{T}_{paz\text{-}asz}\right]^{T}\xi_{asz} \tag{30d}$$

$$\xi_{pmx\text{-}pax}=\xi_{pmx}-\left[\mathbf{T}_{pmx\text{-}pax}\right]^{T}\xi_{pax},\ \xi_{pmy\text{-}pay}=\xi_{pmy}-\left[\mathbf{T}_{pmy\text{-}pay}\right]^{T}\xi_{pay} \text{ and } \xi_{pmz\text{-}paz}=\xi_{pmz}-\left[\mathbf{T}_{pmz\text{-}paz}\right]^{T}\xi_{paz} \tag{31}$$

Suppose that the thickness of the beams and the edge length of the rigid stages are identical, which are represented as t and w, respectively. Additionally, υ is the Poisson ratio of the material, and $\delta=1/(1+\upsilon)$. Based on Eqs. (18) and (27), the variable constraint forces offered by the AM-X, AM-Y, AM-Z, PM-X, PM-Y and PM-Z can be written as shown in Eq. (32).

$$\begin{aligned}&\zeta_{amx}=-\mathrm{K}_{EBeam}\left(\xi_{amx},w,t,\delta\right),\ \zeta_{amy}=-\mathrm{K}_{EBeam}\left(\xi_{amy},w,t,\delta\right),\ \zeta_{amz}=-\mathrm{K}_{EBeam}\left(\xi_{amz},w,t,\delta\right)\\&\zeta_{pmx}=-\mathrm{K}_{FBeam}\left(\xi_{pmx\text{-}pax},w,t,\delta\right),\ \zeta_{pmy}=-\mathrm{K}_{FBeam}\left(\xi_{pmy\text{-}pay},w,t,\delta\right),\ \zeta_{pmz}=-\mathrm{K}_{FBeam}\left(\xi_{pmz\text{-}paz},w,t,\delta\right)\end{aligned} \tag{32}$$

where ζ_{amx}, ζ_{amy}, ζ_{amz}, ζ_{pmx}, ζ_{pmy} and ζ_{pmz} are the variable constraint forces of the AM-X, AM-Y, AM-Z, PM-X, PM-Y and PM-Z in the coordinate systems O_{amx}-$X_{amx}Y_{amx}Z_{amx}$, O_{amy}-$X_{amy}Y_{amy}Z_{amy}$, O_{amz}-$X_{amz}Y_{amz}Z_{amz}$, O_{pmx}-$X_{pmx}Y_{pmx}Z_{pmx}$, O_{pmy}-$X_{pmy}Y_{pmy}Z_{pmy}$ and O_{pmz}-$X_{pmz}Y_{pmz}Z_{pmz}$, respectively. In addition, the ζ_{pmx}, ζ_{pmy} and ζ_{pmz} can also be represented in the coordinate systems O_{pax}-$X_{pax}Y_{pax}Z_{pax}$, O_{pay}-$X_{pay}Y_{pay}Z_{pay}$ and O_{paz}-$X_{paz}Y_{paz}Z_{paz}$, respectively, which can be written as ζ_{pmax}, ζ_{pmay} and ζ_{pmaz}, as shown in Eq. (33).

$$\zeta_{pmax}=\mathbf{T}_{pmx\text{-}apx}\zeta_{pmx},\ \zeta_{pmay}=\mathbf{T}_{pmy\text{-}apy}\zeta_{pmy} \text{ and } \zeta_{pmaz}=\mathbf{T}_{pmz\text{-}apz}\zeta_{pmz} \tag{33}$$

The actuation forces acting on the three ASs and the load force exerted on the MS are defined as constant constraint forces, $\boldsymbol{F}_{asx}$, $\boldsymbol{F}_{asy}$, $\boldsymbol{F}_{asz}$ and $\boldsymbol{F}_{m}$, in the coordinate systems O_{asx}-$X_{asx}Y_{asx}Z_{asx}$, O_{asy}-$X_{asy}Y_{asy}Z_{asy}$, O_{asz}-$X_{asz}Y_{asz}Z_{asz}$ and O_{m}-$X_{m}Y_{m}Z_{m}$, respectively. The constant constraint forces can be written in Eq. (34) based on Eq. (1).

$$\begin{aligned}&\boldsymbol{F}_{asx}=\left[f_{asx\text{-}tx},\ f_{asx\text{-}ty},\ f_{asx\text{-}tz},\ f_{asx\text{-}rx},\ f_{asx\text{-}ry},\ f_{asx\text{-}rz}\right]^{T},\ \boldsymbol{F}_{asy}=\left[f_{asy\text{-}tx},\ f_{asy\text{-}ty},\ f_{asy\text{-}tz},\ f_{asy\text{-}rx},\ f_{asy\text{-}ry},\ f_{asy\text{-}rz}\right]^{T},\\&\boldsymbol{F}_{asz}=\left[f_{asz\text{-}tx},\ f_{asz\text{-}ty},\ f_{asz\text{-}tz},\ f_{asz\text{-}rx},\ f_{asz\text{-}ry},\ f_{asz\text{-}rz}\right]^{T},\ \boldsymbol{F}_{m}=\left[f_{m\text{-}tx},\ f_{m\text{-}ty},\ f_{m\text{-}tz},\ f_{m\text{-}rx},\ f_{m\text{-}ry},\ f_{m\text{-}rz}\right]^{T}\end{aligned} \tag{34}$$

Based on Eq. (11), the force equilibrium equations for the ASs and MS can be written in Eq. (35).

$$\begin{aligned}&\boldsymbol{F}_{asx}+\mathbf{T}_{amx\text{-}asx}\zeta_{amx}+\mathbf{T}_{apx\text{-}asx}\zeta_{pmax}=0\\&\boldsymbol{F}_{asy}+\mathbf{T}_{amy\text{-}asy}\zeta_{amy}+\mathbf{T}_{apy\text{-}asy}\zeta_{pmay}=0\\&\boldsymbol{F}_{asz}+\mathbf{T}_{amz\text{-}asz}\zeta_{amz}+\mathbf{T}_{apz\text{-}asz}\zeta_{pmaz}=0\\&\boldsymbol{F}_{m}+\mathbf{T}_{pmx\text{-}m}\zeta_{pmx}+\mathbf{T}_{pmy\text{-}m}\zeta_{pmy}+\mathbf{T}_{pmz\text{-}m}\zeta_{pmz}=0\end{aligned} \tag{35}$$

If combining Eqs. (17), (18), (26), (27), (A.1) – (A.15) and (30) – (35), the force equilibrium equations of the XYZ CPM can be obtained, which are elaborated in Eqs. (B.1) – (B.60) in Appendix B. The nonlinear force-displacement relationship of the XYZ CPM can be calculated from the force equilibrium equations using commercial software MATHEMATICA. If only linear parts of the variable constraint forces of the PMs and AMs are considered, and let the primary translation displacements in the transformation matrices (in Appendix A) be zero, the linear model of the XYZ CPM can be derived, as shown in Eq. (36).

$$\begin{aligned}&\xi_{m}=\boldsymbol{V}_{m}\left(\boldsymbol{W}_{mx}\boldsymbol{F}_{asx}+\boldsymbol{W}_{my}\boldsymbol{F}_{asy}+\boldsymbol{W}_{mz}\boldsymbol{F}_{asz}+\boldsymbol{F}_{m}\right)\\&\xi_{asx}=\boldsymbol{V}_{x}\left(\boldsymbol{W}_{x}\xi_{m}+\boldsymbol{F}_{asx}\right)\\&\xi_{asy}=\boldsymbol{V}_{y}\left(\boldsymbol{W}_{y}\xi_{m}+\boldsymbol{F}_{asy}\right)\\&\xi_{asz}=\boldsymbol{V}_{z}\left(\boldsymbol{W}_{z}\xi_{m}+\boldsymbol{F}_{asz}\right)\end{aligned} \tag{36}$$

where

$$\boldsymbol{V}_{m}=\left[\boldsymbol{U}_{mx}+\boldsymbol{U}_{my}+\boldsymbol{U}_{mz}\right]^{-1}$$

$$\boldsymbol{W}_{mx}=\mathbf{T}_{pmx\text{-}m}\mathbf{k}_{FBeam\text{-}L}\left[\mathbf{T}_{pmx\text{-}pax}\right]^{T}\left[\mathbf{T}_{pax\text{-}asx}\right]^{T}\boldsymbol{V}_{x}$$

$$\boldsymbol{W}_{my}=\mathbf{T}_{pmy\text{-}m}\mathbf{k}_{FBeam\text{-}L}\left[\mathbf{T}_{pmy\text{-}pay}\right]^{T}\left[\mathbf{T}_{pay\text{-}asy}\right]^{T}\boldsymbol{V}_{y}$$

$$\boldsymbol{W}_{mz}=\mathbf{T}_{pmz\text{-}m}\mathbf{k}_{FBeam\text{-}L}\left[\mathbf{T}_{pmz\text{-}paz}\right]^{T}\left[\mathbf{T}_{paz\text{-}asz}\right]^{T}\boldsymbol{V}_{z}$$

$$\boldsymbol{U}_{mx}=\mathbf{T}_{pmx\text{-}m}\mathbf{k}_{FBeam\text{-}L}\left[\mathbf{T}_{pmx\text{-}m}\right]^{T}-\mathbf{T}_{pmx\text{-}m}\mathbf{k}_{FBeam\text{-}L}\left[\mathbf{T}_{pmx\text{-}pax}\right]^{T}\left[\mathbf{T}_{pax\text{-}asx}\right]^{T}\boldsymbol{V}_{x}\boldsymbol{W}_{x}$$

$$\boldsymbol{U}_{my}=\mathbf{T}_{pmy\text{-}m}\mathbf{k}_{FBeam\text{-}L}\left[\mathbf{T}_{pmy\text{-}m}\right]^{T}-\mathbf{T}_{pmy\text{-}m}\mathbf{k}_{FBeam\text{-}L}\left[\mathbf{T}_{pmy\text{-}pay}\right]^{T}\left[\mathbf{T}_{pay\text{-}asy}\right]^{T}\boldsymbol{V}_{y}\boldsymbol{W}_{y}$$

$$\boldsymbol{U}_{mz}=\mathbf{T}_{pmz\text{-}m}\mathbf{k}_{FBeam\text{-}L}\left[\mathbf{T}_{pmz\text{-}m}\right]^{T}-\mathbf{T}_{pmz\text{-}m}\mathbf{k}_{FBeam\text{-}L}\left[\mathbf{T}_{pmz\text{-}paz}\right]^{T}\left[\mathbf{T}_{paz\text{-}asz}\right]^{T}\boldsymbol{V}_{z}\boldsymbol{W}_{z}$$

$$\boldsymbol{U}_{x}=\mathbf{T}_{amx\text{-}asx}\mathbf{k}_{EBeam\text{-}L}\left[\mathbf{T}_{amx\text{-}asx}\right]^{T}+\mathbf{T}_{pax\text{-}asx}\mathbf{T}_{pmx\text{-}pax}\mathbf{k}_{FBeam\text{-}L}\left[\mathbf{T}_{pmx\text{-}pax}\right]^{T}\left[\mathbf{T}_{pax\text{-}asx}\right]^{T}$$

$$\boldsymbol{V}_{x}=\left[\boldsymbol{U}_{x}\right]^{-1}$$

$$\boldsymbol{W}_{x}=\mathbf{T}_{pax\text{-}asx}\mathbf{T}_{pmx\text{-}pax}\mathbf{k}_{FBeam\text{-}L}\left[\mathbf{T}_{pmx\text{-}m}\right]^{T}$$

$$\boldsymbol{U}_{\mathrm{y}}=\mathbf{T}_{\text{amy-asy}}\mathbf{k}_{\text{EBeam-L}}\left[\mathbf{T}_{\text{amy-asy}}\right]^{\mathrm{T}}+\mathbf{T}_{\text{pay-asy}}\mathbf{T}_{\text{pmy-pay}}\mathbf{k}_{\text{FBeam-L}}\left[\mathbf{T}_{\text{pmy-pay}}\right]^{\mathrm{T}}\left[\mathbf{T}_{\text{pay-asy}}\right]^{\mathrm{T}}$$

$$\boldsymbol{V}_{\mathrm{y}}=\left[\boldsymbol{U}_{\mathrm{y}}\right]^{-1}$$

$$\boldsymbol{W}_{\mathrm{y}}=\mathbf{T}_{\text{pay-asy}}\mathbf{T}_{\text{pmy-pay}}\mathbf{k}_{\text{FBeam-L}}\left[\mathbf{T}_{\text{pmy-m}}\right]^{\mathrm{T}}$$

$$\boldsymbol{U}_{\mathrm{z}}=\mathbf{T}_{\text{amz-asz}}\mathbf{k}_{\text{EBeam-L}}\left[\mathbf{T}_{\text{amz-asz}}\right]^{\mathrm{T}}+\mathbf{T}_{\text{paz-asz}}\mathbf{T}_{\text{pmz-paz}}\mathbf{k}_{\text{FBeam-L}}\left[\mathbf{T}_{\text{pmz-paz}}\right]^{\mathrm{T}}\left[\mathbf{T}_{\text{paz-asz}}\right]^{\mathrm{T}}$$

$$\boldsymbol{V}_{\mathrm{z}}=\left[\boldsymbol{U}_{\mathrm{z}}\right]^{-1}$$

$$\boldsymbol{W}_{\mathrm{z}}=\mathbf{T}_{\text{paz-asz}}\mathbf{T}_{\text{pmz-paz}}\mathbf{k}_{\text{FBeam-L}}\left[\mathbf{T}_{\text{pmz-m}}\right]^{\mathrm{T}}$$

The following results can be derived from the linear and nonlinear analytical models of the XYZ CPM (the linear analytical model is valid for very small motion range): (a) the displacements of the MS under the influence of specific external forces, (b) the displacements of the AS-X, AS-Y and AS-Z under the influence of specific external forces, (c) the lost motions between the displacements of the MS and the displacements of the AS-X, AS-Y and AS-Z, (d) the actuation stiffness along the X_m-, Y_m- and Z-axes, and (e) the relationships between the displacements and the geometric parameters. In addition, the analytical models can also be employed to optimize XYZ CPM as studied in [31]. The motion performance analysis of the XYZ CPM will be our future work.

6 FEA Simulations and Experimental Tests

In this section, a series of FEA simulations and experimental tests are carried out to validate the linear and nonlinear analytical models of the XYZ CPM.

6.1 FEA Simulations

For the FEA model of the XYZ CPM, let the beam's length, L, be 50mm, the beam's thickness, t, be 1mm, the edge's length, w, of the rigid stages be 25mm, the Poisson's ratio, υ, be 0.33, and the Young's modulus, E, be 6.9×10^{10}Pa. Commercial software, COMSOL MULTIPHYSICS, is selected for the nonlinear FEA simulations, using the 10-node tetrahedral element and extra fine meshing technology (maximum element size 3.5 mm, minimum element size 0.15 mm, maximum element growth rate 1.35, curvature factor 0.3, and resolution of narrow regions 0.85). The XYZ CPM is actuated by three linear translational actuators without considering the mass of the XYZ CPM. Therefore, the constant constraint forces, F_{asx}, F_{asy}, F_{asz} and F_{m}, can be simplified, as shown in Eq. (37).

$$\boldsymbol{F}_{\text{asx}}=\left[f_{\text{asx-tx}},\,0,\,0,\,0,\,0,\,0\right]^{\mathrm{T}},\ \boldsymbol{F}_{\text{asy}}=\left[f_{\text{asy-tx}},\,0,\,0,\,0,\,0,\,0\right]^{\mathrm{T}},\ \boldsymbol{F}_{\text{asz}}=\left[f_{\text{asz-tx}},\,0,\,0,\,0,\,0,\,0\right]^{\mathrm{T}}\text{ and }\boldsymbol{F}_{\text{m}}=\left[0,\,0,\,0,\,0,\,0,\,0\right]^{\mathrm{T}} \tag{37}$$

In order to achieve a $\pm0.1L$ motion range per axis (the motion range can be considered as an medium large motion range compared with the length of the beam [44]), the actuation force per axis varies from −40N to +40N. The designed XYZ CPM has an isotropic configuration, so the model, associated with the motions of the MS and AS-X, is validated under the following conditions: (a) $f_{\text{asx-tx}}$ varies from −40N to +40N when $f_{\text{asy-tx}}$=0 and $f_{\text{asz-tx}}$=0, (b) $f_{\text{asx-tx}}$ varies from −40N to +40N when $f_{\text{asy-tx}}$=40N and $f_{\text{asz-tx}}$=0, and (c) $f_{\text{asx-tx}}$ varies from −40N to +40N when $f_{\text{asy-tx}}$=40N and $f_{\text{asz-tx}}$=40N. The nonlinear FEA results, nonlinear analytical results and linear analytical results can be seen in Figs. 7 and 8.

It can be seen from Fig. 7 that the nonlinear analytical results match the FEA results well, and the linear analytical results have small difference compared with the FEA results within small motion ranges. For the translations of the MS, the difference between the FEA results and the nonlinear results is less than 3.25% in the translations along the X_m- and Y_m-axes (Figs. 7(a) and 7(b)), and less than 4.92% in the translation along the Z_m-axis (Fig. 7(c)). The difference between the FEA results and the linear results is less than 6.59% in the translations along the X_m- and Y_m-axes (Figs. 7(a) and 7(b)), and less than 13.48% in the translation along the Z_m-axis (Fig. 7(c)). For the results of the MS's rotations about the Y_m- and Z_m-axes, as shown in Figs. 7(e) and 7(f), the maximum difference between the FEA results and the nonlinear results is less than 2.7% under all the conditions, while the maximum difference between the FEA results and the linear results is about 16.3%. Compared with the FEA results, the linear and nonlinear results of the rotations about the X_m-axis, as shown in Fig. 7(d), have larger difference, because the results (in the order of 10^{-4} rad) shown in this figure are comparable to the simulation accuracy and the analytical approximations. However, the analytical results of the rotations about the X_m-axis still have similar trends as that of associated FEA results.

Figure 7(a) also shows that the translations of the MS along the X-axis among the different conditions have small differences, which means that the translation of the MS along the X-axis is almost decoupled from the translations of the MS along the other two directions. Figures 7(b) and 7(c) illustrate that the translations of the MS along the Y_m- and Z_m-axes are insensitive to the force along the X_m-axis, which also validates the cross-axis decoupling motion characteristics. Other motion characteristics, such as lost motion and actuation stiffness, of the XYZ CPM can also be captured from the linear and nonlinear models, which are not detailed in Fig. 7.

Figure 8 illustrates that the nonlinear analytical results of the AS-X's translations have small difference compared with the FEA results, which are less than 2.74% in the translation along the X_m-axis (Fig. 8(a)), less than 5.33% in the translation along the Y_m-axis (Fig. 8(b)), and less than 4.55% in the translation along the Z_m-axis (Fig. 8(c)). But the linear results have a little larger difference compared with the FEA results, because the linear results cannot capture the elastokinematic effects [16]. For the rotations of the AS-X, the maximum difference between the FEA results and the analytical results occurs in the rotations about the

X_m-axis (Fig. 8(d)) mainly due to their tiny values (in the order of 10^{-5} rad) which are close to the simulation accuracy and the analytical approximations, but the nonlinear analytical results have similar trends as the FEA results. The parasitic rotations of the AS-X about the Y_m- and Z_m-axes can be seen from Figs. 8(e) – 8(f), showing that the nonlinear results have maximum about 7% difference compared with the FEA results. Figure 8(a) also shows that the translation of the AS-X along the X_m-axis in the different conditions is almost decoupled from the primary translations of the AS-Y and AS-Z.

The small difference between the nonlinear results and FEA results mainly arises from the approximation in deriving the analytical model as well as the errors of the FEA simulations. The FEA simulations have errors, especially when the results are close to the relative repair tolerance of the software (10^{-6} mm for the simulations in this paper). The linear analytical results, with a particular emphasis on the results in terms of the primary translations, also have acceptable differences within small motion ranges compared with the FEA results.

6.2 Experimental Tests

The assembled prototype of the XYZ CPM (as shown in Fig. 9) is made of Aluminum 99.5, whose Yield strength is approximately 105MPa. Additionally, the Poisson's ratio, Young's modulus and geometric dimensions are the same as the values in the FEA simulation in Sec. 6.1. The maximum motion range per axis should be less than 0.634mm (about 5N actuation force per axis) as calculated in Eq. (38) based on [45]. The following conditions are considered in this experimental validation: (a) $f_{\text{asx-tx}}$ varies from 0 to 5N when $f_{\text{asy-tx}}$=0 and $f_{\text{asz-tx}}$=0, (b) $f_{\text{asx-tx}}$ varies from 0 to 5N when $f_{\text{asy-tx}}$=4.2826N and $f_{\text{asz-tx}}$=0, and (c) $f_{\text{asx-tx}}$ varies from 0 to 5N when $f_{\text{asy-tx}}$=4.2826N and $f_{\text{asz-tx}}$=−4.890N.

$$\text{Motion Range} \le 0.1667\frac{\sigma_s}{Et^2}=0.1667\times\frac{105\text{MPa}}{6.9\times10^{10}\,\text{Pa}\times\left(\frac{1\text{mm}}{50\,\text{mm}}\right)^2}=0.634\text{mm} \tag{38}$$

The displacements of the MS along the X_m- and Y_m-axes are measured by two digital dial gauges with 0.001mm resolution. The actuation forces are conducted by mass blocks, the mass of which are measured by an electronic scale with 0.001g resolution. Note that the displacements of the MS along the X_m- and Y_m-axes are measured not on the top center of the MS but on the surfaces as shown in Fig. 9. Additionally, only the rotational displacement of the MS about the Z_m-axis is considered in this experimental test. A low-cost method of measuring this tiny rotational displacement is figured out in this paper, the principle of which is indicated, as shown in Fig. 10.

As shown in Fig. 10, the rotation angle can be calculated as shown in Eq. (39). If δ_{ny} are much smaller than D_{LB}, Equation (39) can be simplified to Eq. (40).

$$\alpha_{\text{LB}}=\arctan\left(\frac{d_{\text{LB}}-\delta_{\text{nx}}}{D_{\text{LB}}-\delta_{\text{ny}}}\right) \tag{39}$$

$$\alpha_{\text{LB}}\approx\arctan\left(\frac{d_{\text{LB}}-\delta_{\text{nx}}}{D_{\text{LB}}}\right) \tag{40}$$

In this experimental test, the rotational displacement of the MS about the Z_m-axis is obtained based on the equation above. More specifically, as shown in Fig. 11(a), a laser pointer is fixed on the MS, so the laser pointer has the same displacements as the MS. At a long distance away from the laser pointer (6800mm in this case), a screen shown in Fig. 11(b) is pasted onto a wall. At first, let the laser beam be vertical to the screen, and mark the position of the original laser spot on the screen using a HD camera, as shown in Fig. 11(b). When the MS moves to new positions under actuation forces, the HD camera records the new positions of the laser spots. Therefore, a series of pictures of the laser spots, such as the pictures shown in Figs. 11(c) – 11(h), are obtained. The positions of the laser spots on the pictures are figured out using image processing function of MATLAB software. Based on the positions and Eq. (40), the rotational angles of the MS about the Z_m-axis are obtained over the different conditions.

Figure 12(a) shows that the translations of the MS along the X-axis in the different conditions. The nonlinear analytical results have tiny difference compared with the FEA results (less than 2.73%), and have acceptable small difference compared with the experiment results (less than 8.98%). It can be seen from Figs. 12(c) and 12(d) that the nonlinear analytical results have small differences compared with the FEA results and the experiment results, the maximum difference is about 2.79%. Figure 12(b) shows that the analytical results have larger difference compared with the FEA results and the experiment results, because the displacements shown in this figure are close to the manufacture and experiment errors and the simulation accuracy. However, the analytical, FEA and experiment results have the similar trends.

The rotations of the MS about the Z-axis in the different conditions are illustrated in Fig. 13. It can be seen that the nonlinear analytical results match the FEA results well, and the maximum difference is less than 5.2%. The difference between the nonlinear analytical results and the experiment results is a little larger mainly due to the manufacture and experiment errors, but the nonlinear analytical results and the experiment results follow the similar trends. The difference among the FEA, analytical and experiment results arises mainly from the following issues: FEA simulation error, manufacture error, assembly error, experiment error, and data processing error (i.e. the positioning errors of the laser spots on the screen identified using MATLAB image processing function).

7 Conclusions

This paper has proposed a CFB modelling approach for modelling compliant mechanisms. The CFB modelling approach decomposes a compliant mechanism into rigid stages and compliant modules. The compliant modules can be basic compliant modules and non-basic compliant modules. The derivation of the variable constraint forces produced by the basic compliant modules and non-basic compliant modules was detailed in this paper. External constraint forces such as actuation forces were defined as constant constraint forces. The constraint force equilibrium equations of a balanced compliant mechanism can be represented by such variable constraint forces and constant constraint forces, and then the analytical model of the compliant mechanism can be derived from the constraint force equilibrium equations. In this paper, the variable constraint force of a wire beam was obtained, which was used to derive the variable constraint forces of a four-beam non-basic compliant module and an eight-beam non-basic compliant module. Furthermore, an XYZ CPM was analytically modelled based on the derived variable constraint forces of the two types of non-basic compliant modules using the CFB modelling approach. The analytical model of the XYZ CPM was also validated by both FEA simulations and experimental tests.

The proposed CFB modelling approach is an improvement of the FBD-based modelling approach and a development of screw-theory-based design approach. The mathematical expressions in the CFB modelling approach have an easily understood physical meaning, and dynamic effects of a compliant mechanism can also be considered in the CFB modelling approach. Unlike the screw-theory-based design approach, the CFB modelling approach can take the exact constraint forces of compliant modules into account.

The CFB modelling approach can be further extended to an approach for optimizing compliant mechanisms. Each compliant module in a compliant mechanism has a great number of possible permitted positions, and the set of all the possible permitted positions is the position space of the compliant module in the compliant mechanism. Based on this position space concept, a compliant mechanism can be reconfigured into a series of new compliant mechanisms. If a compliant mechanism termed 'Compliant Mechanism-Original' is modelled using the CFB modelling approach, the compliant mechanisms reconfigured from the Compliant Mechanism-Original can also be modelled easily, via only modifying the transformation matrices. On the other hand, a compliant mechanism with desired motion performance can be obtained through optimizing the transformation matrices (the same as optimizing the positions of the compliant modules). Therefore, the CFB modelling approach can also be easily employed to optimize compliant mechanisms.

ACKNOWLEDGMENT

The authors would like to express their greatest gratitude to Irish Research Council (IRC) for awarding an IRCSET Embark PhD scholarship (RS/2012/361) to Mr. Haiyang Li. The authors would also like to greatly acknowledge the help of Mr. Timothy Power and Mr. Michael O'Shea. The fabrication of the prototype would have been impossible without the unconditional help offered by them.

Appendix A: Transformation Matrices for the XYZ CPM Modelling

$$\mathbf{T}_{\text{pax-pmx}}=\begin{bmatrix} 1 & 0 & 0 & 0 & 0 & 0 \\ 0 & 1 & 0 & 0 & 0 & 0 \\ 0 & 0 & 1 & 0 & 0 & 0 \\ 0 & \xi_{\text{m-tz}} & -\xi_{\text{m-ty}} & 1 & 0 & 0 \\ -\xi_{\text{m-tz}} & 0 & -\xi_{\text{asx-tx}}+\xi_{\text{m-tx}}+1 & 0 & 1 & 0 \\ \xi_{\text{m-ty}} & \xi_{\text{asx-tx}}-\xi_{\text{m-tx}}-1 & 0 & 0 & 0 & 1 \end{bmatrix} \quad \text{(A.1)}$$

$$\mathbf{T}_{\text{pay-pmy}}=\begin{bmatrix} 1 & 0 & 0 & 0 & 0 & 0 \\ 0 & 1 & 0 & 0 & 0 & 0 \\ 0 & 0 & 1 & 0 & 0 & 0 \\ 0 & \xi_{\text{m-tx}} & -\xi_{\text{m-tz}} & 1 & 0 & 0 \\ -\xi_{\text{m-tx}} & 0 & -\xi_{\text{asy-tx}}+\xi_{\text{m-ty}}+1 & 0 & 1 & 0 \\ \xi_{\text{m-tz}} & \xi_{\text{asy-tx}}-\xi_{\text{m-ty}}-1 & 0 & 0 & 0 & 1 \end{bmatrix} \quad \text{(A.2)}$$

$$\mathbf{T}_{\text{paz-pmz}}=\begin{bmatrix} 1 & 0 & 0 & 0 & 0 & 0 \\ 0 & 1 & 0 & 0 & 0 & 0 \\ 0 & 0 & 1 & 0 & 0 & 0 \\ 0 & \xi_{\text{m-ty}} & -\xi_{\text{m-tx}} & 1 & 0 & 0 \\ -\xi_{\text{m-ty}} & 0 & -\xi_{\text{asz-tx}}+\xi_{\text{m-tz}}+1 & 0 & 1 & 0 \\ \xi_{\text{m-tx}} & \xi_{\text{asz-tx}}-\xi_{\text{m-tz}}-1 & 0 & 0 & 0 & 1 \end{bmatrix} \quad \text{(A.3)}$$

$$\mathbf{T}_{\text{pmz-m}}=\begin{bmatrix} 0 & 1 & 0 & 0 & 0 & 0 \\ 0 & 0 & 1 & 0 & 0 & 0 \\ 1 & 0 & 0 & 0 & 0 & 0 \\ 0 & 0 & w & 0 & 1 & 0 \\ 0 & -w & 0 & 0 & 0 & 1 \\ 0 & 0 & 0 & 1 & 0 & 0 \end{bmatrix} \quad \text{(A.9)}$$

$$\mathbf{T}_{\text{pax-asx}}=\begin{bmatrix} 1 & 0 & 0 & 0 & 0 & 0 \\ 0 & 1 & 0 & 0 & 0 & 0 \\ 0 & 0 & 1 & 0 & 0 & 0 \\ 0 & 0 & 0 & 1 & 0 & 0 \\ 0 & 0 & -w & 0 & 1 & 0 \\ 0 & w & 0 & 0 & 0 & 1 \end{bmatrix} \quad \text{(A.10)}$$

$$\mathbf{T}_{\text{pay-asy}}=\begin{bmatrix} 1 & 0 & 0 & 0 & 0 & 0 \\ 0 & 1 & 0 & 0 & 0 & 0 \\ 0 & 0 & 1 & 0 & 0 & 0 \\ 0 & 0 & 0 & 1 & 0 & 0 \\ 0 & 0 & -w & 0 & 1 & 0 \\ 0 & w & 0 & 0 & 0 & 1 \end{bmatrix} \quad \text{(A.11)}$$

$$\mathbf{T}_{\text{pmx-pax}}=\begin{bmatrix}1 & 0 & 0 & 0 & 0 & 0\\ 0 & 1 & 0 & 0 & 0 & 0\\ 0 & 0 & 1 & 0 & 0 & 0\\ 0 & -\xi_{\text{m-tz}} & \xi_{\text{m-ty}} & 1 & 0 & 0\\ \xi_{\text{m-tz}} & 0 & \xi_{\text{asx-tx}}-\xi_{\text{m-tx}}-1 & 0 & 1 & 0\\ -\xi_{\text{m-ty}} & -\xi_{\text{asx-tx}}+\xi_{\text{m-tx}}+1 & 0 & 0 & 0 & 1\end{bmatrix} \quad \text{(A.4)}$$

$$\mathbf{T}_{\text{pmy-pay}}=\begin{bmatrix}1 & 0 & 0 & 0 & 0 & 0\\ 0 & 1 & 0 & 0 & 0 & 0\\ 0 & 0 & 1 & 0 & 0 & 0\\ 0 & -\xi_{\text{m-tx}} & \xi_{\text{m-tz}} & 1 & 0 & 0\\ \xi_{\text{m-tx}} & 0 & \xi_{\text{asy-tx}}-\xi_{\text{m-ty}}-1 & 0 & 1 & 0\\ -\xi_{\text{m-tz}} & -\xi_{\text{asy-tx}}+\xi_{\text{m-ty}}+1 & 0 & 0 & 0 & 1\end{bmatrix} \quad \text{(A.5)}$$

$$\mathbf{T}_{\text{pmz-paz}}=\begin{bmatrix}1 & 0 & 0 & 0 & 0 & 0\\ 0 & 1 & 0 & 0 & 0 & 0\\ 0 & 0 & 1 & 0 & 0 & 0\\ 0 & -\xi_{\text{m-ty}} & \xi_{\text{m-tx}} & 1 & 0 & 0\\ \xi_{\text{m-ty}} & 0 & \xi_{\text{asz-tx}}-\xi_{\text{m-tz}}-1 & 0 & 1 & 0\\ -\xi_{\text{m-tx}} & -\xi_{\text{asz-tx}}+\xi_{\text{m-tz}}+1 & 0 & 0 & 0 & 1\end{bmatrix} \quad \text{(A.6)}$$

$$\mathbf{T}_{\text{pmx-m}}=\begin{bmatrix}1 & 0 & 0 & 0 & 0 & 0\\ 0 & 1 & 0 & 0 & 0 & 0\\ 0 & 0 & 1 & 0 & 0 & 0\\ 0 & w/2 & 0 & 1 & 0 & 0\\ -w/2 & 0 & w/2 & 0 & 1 & 0\\ 0 & -w/2 & 0 & 0 & 0 & 1\end{bmatrix} \quad \text{(A.7)}$$

$$\mathbf{T}_{\text{pmy-m}}=\begin{bmatrix}0 & 0 & 1 & 0 & 0 & 0\\ 1 & 0 & 0 & 0 & 0 & 0\\ 0 & 1 & 0 & 0 & 0 & 0\\ w/2 & -w/2 & 0 & 0 & 0 & 1\\ 0 & 0 & -w/2 & 1 & 0 & 0\\ 0 & 0 & w/2 & 0 & 1 & 0\end{bmatrix} \quad \text{(A.8)}$$

$$\mathbf{T}_{\text{paz-asz}}=\begin{bmatrix}1 & 0 & 0 & 0 & 0 & 0\\ 0 & 1 & 0 & 0 & 0 & 0\\ 0 & 0 & 1 & 0 & 0 & 0\\ 0 & 0 & 0 & 1 & 0 & 0\\ 0 & 0 & -w & 0 & 1 & 0\\ 0 & w & 0 & 0 & 0 & 1\end{bmatrix} \quad \text{(A.12)}$$

$$\mathbf{T}_{\text{amx-asx}}=\begin{bmatrix}1 & 0 & 0 & 0 & 0 & 0\\ 0 & 1 & 0 & 0 & 0 & 0\\ 0 & 0 & 1 & 0 & 0 & 0\\ 0 & 0 & 0 & 1 & 0 & 0\\ 0 & 0 & -w/2 & 0 & 1 & 0\\ 0 & w/2 & 0 & 0 & 0 & 1\end{bmatrix} \quad \text{(A.13)}$$

$$\mathbf{T}_{\text{amy-asy}}=\begin{bmatrix}1 & 0 & 0 & 0 & 0 & 0\\ 0 & 1 & 0 & 0 & 0 & 0\\ 0 & 0 & 1 & 0 & 0 & 0\\ 0 & 0 & 0 & 1 & 0 & 0\\ 0 & 0 & -w/2 & 0 & 1 & 0\\ 0 & w/2 & 0 & 0 & 0 & 1\end{bmatrix} \quad \text{(A.14)}$$

$$\mathbf{T}_{\text{amz-asz}}=\begin{bmatrix}1 & 0 & 0 & 0 & 0 & 0\\ 0 & 1 & 0 & 0 & 0 & 0\\ 0 & 0 & 1 & 0 & 0 & 0\\ 0 & 0 & 0 & 1 & 0 & 0\\ 0 & 0 & -w/2 & 0 & 1 & 0\\ 0 & w/2 & 0 & 0 & 0 & 1\end{bmatrix} \quad \text{(A.15)}$$

where w is the edge length of the rigid stages. $\xi_{\text{m-tx}}$, $\xi_{\text{m-ty}}$ and $\xi_{\text{m-tz}}$ are the three of the six entries of $\boldsymbol{\xi}_{\text{m}}$, which are used to represent the translations of the MS along the X_m-, Y_m- and Z_m-axes, respectively. $\xi_{\text{asx-tx}}$, $\xi_{\text{asy-tx}}$ and $\xi_{\text{asz-tx}}$ are the X-direction translational displacements of the AS-X, AS-Y and AS-Z in their own local coordinate systems, respectively. The translations of the MS and the X-axis translations of the AS-X, AS-Y and AS-Z are the primary translations of the XYZ CPM. The other translations and rotations of the MS, AS-X, AS-Y and AS-Z are the parasitic motions of the XYZ CPM. The parasitic motions are much smaller than the primary translations, so the parasitic motions are not taken into account in the transformation matrices. If let the primary translations, $\xi_{\text{m-tx}}$, $\xi_{\text{m-ty}}$, $\xi_{\text{m-tz}}$, $\xi_{\text{asx-tx}}$, $\xi_{\text{asy-tx}}$ and $\xi_{\text{asz-tx}}$, in the transformation matrices be zero, the transformation matrices above can be simplified to linear transformation matrices of the XYZ CPM corresponding to the un-deformed configuration of the XYZ CPM.

Appendix B: Nonlinear Constraint Force Equilibrium Equations of the XYZ CPM

$$\zeta_{\text{pmx-tx}}=\frac{1680\left(5\left(\xi_{\text{m-tx}}-\xi_{\text{asx-tx}}\right)+3\left(\left(\xi_{\text{m-ty}}-\xi_{\text{asx-ty}}\right)^2+\left(\xi_{\text{m-tz}}-\xi_{\text{asx-tz}}\right)^2\right)\right)}{3\left(\xi_{\text{m-ty}}-\xi_{\text{asx-ty}}\right)^2+3\left(\xi_{\text{m-tz}}-\xi_{\text{asx-tz}}\right)^2+175t^2} \quad \text{(B.1)}$$

$$\zeta_{\text{pmx-ty}}=\left(48\left(\xi_{\text{m-ty}}-\xi_{\text{asx-ty}}\right)\left(210\left(\xi_{\text{m-tx}}-\xi_{\text{asx-tx}}\right)+129\left(\xi_{\text{m-ty}}-\xi_{\text{asx-ty}}\right)^2+129\left(\xi_{\text{m-tz}}-\xi_{\text{asx-tz}}\right)^2+175t^2\right)\right)/\left(3\left(\xi_{\text{m-ty}}-\xi_{\text{asx-ty}}\right)^2+3\left(\xi_{\text{m-tz}}-\xi_{\text{asx-tz}}\right)^2+175t^2\right) \quad \text{(B.2)}$$

$$\zeta_{\text{pmx-tz}}=\left(48\left(\xi_{\text{m-tz}}-\xi_{\text{asx-tz}}\right)\left(210\left(\xi_{\text{m-tx}}-\xi_{\text{asx-tx}}\right)+129\left(\xi_{\text{m-ty}}-\xi_{\text{asx-ty}}\right)^2+129\left(\xi_{\text{m-tz}}-\xi_{\text{asx-tz}}\right)^2+175t^2\right)\right)/\left(3\left(\xi_{\text{m-ty}}-\xi_{\text{asx-ty}}\right)^2+3\left(\xi_{\text{m-tz}}-\xi_{\text{asx-tz}}\right)^2+175t^2\right) \quad \text{(B.3)}$$

$$\zeta_{\mathrm{pmx-rx}}=4\left(\begin{array}{l}\delta\left(\xi_{\mathrm{m-rx}}-\xi_{\mathrm{asx-rx}}\right)\left(3\left(\xi_{\mathrm{m-ty}}-\xi_{\mathrm{asx-ty}}\right)^2+3\left(\xi_{\mathrm{m-tz}}-\xi_{\mathrm{asx-tz}}\right)^2+175t^2\right)\\-210\left(5t^2-3tw+3w^2\right)\left(\left(\xi_{\mathrm{m-ry}}-\xi_{\mathrm{asx-ry}}\right)\left(\xi_{\mathrm{m-ty}}-\xi_{\mathrm{asx-ty}}\right)+\left(\xi_{\mathrm{m-rz}}-\xi_{\mathrm{asx-rz}}\right)\left(\xi_{\mathrm{m-tz}}-\xi_{\mathrm{asx-tz}}\right)\right)\end{array}\right)/\left(3\left(\xi_{\mathrm{m-ty}}-\xi_{\mathrm{asx-ty}}\right)^2+3\left(\xi_{\mathrm{m-tz}}-\xi_{\mathrm{asx-tz}}\right)^2+175t^2\right) \tag{B.4}$$

$$\zeta_{\mathrm{pmx-ry}}=4\left(\begin{array}{l}175\left(4t^2-3tw+3w^2\right)\left(\xi_{\mathrm{m-ry}}-\xi_{\mathrm{asx-ry}}\right)\\+6\left(\xi_{\mathrm{m-tz}}-\xi_{\mathrm{asx-tz}}\right)\left(35\left(\xi_{\mathrm{m-tx}}-\xi_{\mathrm{asx-tx}}\right)+24\left(\xi_{\mathrm{m-ty}}-\xi_{\mathrm{asx-ty}}\right)^2+24\left(\xi_{\mathrm{m-tz}}-\xi_{\mathrm{asx-tz}}\right)^2+175t^2\right)\end{array}\right)/\left(3\left(\xi_{\mathrm{m-ty}}-\xi_{\mathrm{asx-ty}}\right)^2+3\left(\xi_{\mathrm{m-tz}}-\xi_{\mathrm{asx-tz}}\right)^2+175t^2\right) \tag{B.5}$$

$$\zeta_{\mathrm{pmx-rz}}=4\left(\begin{array}{l}175\left(4t^2-3tw+3w^2\right)\left(\xi_{\mathrm{m-rz}}-\xi_{\mathrm{asx-rz}}\right)\\-6\left(\xi_{\mathrm{m-ty}}-\xi_{\mathrm{asx-ty}}\right)\left(35\left(\xi_{\mathrm{m-tx}}-\xi_{\mathrm{asx-tx}}\right)+24\left(\xi_{\mathrm{m-ty}}-\xi_{\mathrm{asx-ty}}\right)^2+24\left(\xi_{\mathrm{m-tz}}-\xi_{\mathrm{asx-tz}}\right)^2+175t^2\right)\end{array}\right)/\left(3\left(\xi_{\mathrm{m-ty}}-\xi_{\mathrm{asx-ty}}\right)^2+3\left(\xi_{\mathrm{m-tz}}-\xi_{\mathrm{asx-tz}}\right)^2+175t^2\right) \tag{B.6}$$

$$\zeta_{\mathrm{amx-tx}}=\frac{96\xi_{\mathrm{asx-tx}}\left(35\left(3\left(\xi_{\mathrm{asx-tz}}-\frac{1}{2}w\xi_{\mathrm{asx-ry}}\right)+3\left(\frac{1}{2}w\xi_{\mathrm{asx-rz}}+\xi_{\mathrm{asx-ty}}\right)+5t^2\right)+129\xi_{\mathrm{asx-tx}}^2\right)}{3\xi_{\mathrm{asx-tx}}^2+175t^2} \tag{B.7}$$

$$\zeta_{\mathrm{amx-ty}}=\frac{1}{3\xi_{\mathrm{asx-tx}}^2+175t^2}24\left(\begin{array}{l}w\xi_{\mathrm{asx-rx}}\left(35\left(6\left(\xi_{\mathrm{asx-tz}}-\frac{1}{2}w\xi_{\mathrm{asx-ry}}\right)+5t^2\right)+129\xi_{\mathrm{asx-tx}}^2\right)\\+70\left(\frac{1}{2}w\xi_{\mathrm{asx-rz}}+\xi_{\mathrm{asx-ty}}\right)\left(6\left(\xi_{\mathrm{asx-tz}}-\frac{1}{2}w\xi_{\mathrm{asx-ry}}\right)+5t^2+5\right)+6\xi_{\mathrm{asx-tx}}^2\left(43\left(\frac{1}{2}w\xi_{\mathrm{asx-rz}}+\xi_{\mathrm{asx-ty}}\right)+35\right)\end{array}\right) \tag{B.8}$$

$$\zeta_{\mathrm{amx-tz}}=-\frac{1}{3\xi_{\mathrm{asx-tx}}^2+175t^2}24\left(\begin{array}{l}w\xi_{\mathrm{asx-rx}}\left(35\left(6\left(\frac{1}{2}w\xi_{\mathrm{asx-rz}}+\xi_{\mathrm{asx-ty}}\right)+5t^2\right)+129\xi_{\mathrm{asx-tx}}^2\right)\\-2\left(35\left(\xi_{\mathrm{asx-tz}}-\frac{1}{2}w\xi_{\mathrm{asx-ry}}\right)\left(6\left(\frac{1}{2}w\xi_{\mathrm{asx-rz}}+\xi_{\mathrm{asx-ty}}\right)+5t^2+5\right)+3\xi_{\mathrm{asx-tx}}^2\left(43\left(\xi_{\mathrm{asx-tz}}-\frac{1}{2}w\xi_{\mathrm{asx-ry}}\right)+35\right)\right)\end{array}\right) \tag{B.9}$$

$$\zeta_{\mathrm{amx-rx}}=\frac{1}{3\xi_{\mathrm{asx-tx}}^2+175t^2}4\left(\begin{array}{l}\xi_{\mathrm{asx-rx}}\left(35\left(\begin{array}{l}3w\left(6w+1\right)\left(\xi_{\mathrm{asx-tz}}-\frac{1}{2}w\xi_{\mathrm{asx-ry}}\right)+3w\left(6w+1\right)\left(\frac{1}{2}w\xi_{\mathrm{asx-rz}}+\xi_{\mathrm{asx-ty}}\right)\\+10\left(t^2\left(3w^2+3w+4\right)-3tw+3w^2\right)\end{array}\right)+18w\left(43w+8\right)\xi_{\mathrm{asx-tx}}^2\right)\\+6\left(3\left(43w+8\right)\xi_{\mathrm{asx-tx}}^2+175t^2\left(w+1\right)\right)\left(\frac{1}{2}w\xi_{\mathrm{asx-ry}}+\frac{1}{2}w\xi_{\mathrm{asx-rz}}+\xi_{\mathrm{asx-ty}}-\xi_{\mathrm{asx-tz}}\right)\end{array}\right) \tag{B.10}$$

$$\zeta_{\mathrm{amx-ry}}=-\frac{1}{3\xi_{\mathrm{asx-tx}}^2+175t^2}4\left(\begin{array}{l}6\xi_{\mathrm{asx-tx}}\left(35\left(5t^2-3tw+3w^2\right)\xi_{\mathrm{asx-rx}}+35\left(\left(6w+1\right)\left(\xi_{\mathrm{asx-tz}}-\frac{1}{2}w\xi_{\mathrm{asx-ry}}\right)+5t^2\left(w+1\right)\right)+3\left(43w+8\right)\xi_{\mathrm{asx-tx}}^2\right)\\-\xi_{\mathrm{asx-ry}}\left(3\delta\xi_{\mathrm{asx-tx}}^2+175\left(\left(\delta+4\right)t^2-3tw+3w^2\right)\right)\end{array}\right) \tag{B.11}$$

$$\zeta_{\mathrm{amx-rz}}=\frac{1}{3\xi_{\mathrm{asx-tx}}^2+175t^2}4\left(\begin{array}{l}6\xi_{\mathrm{asx-tx}}\left(-35\left(5t^2-3tw+3w^2\right)\xi_{\mathrm{asx-rx}}+35\left(\left(6w+1\right)\left(\frac{1}{2}w\xi_{\mathrm{asx-rz}}+\xi_{\mathrm{asx-ty}}\right)+5t^2\left(w+1\right)\right)+3\left(43w+8\right)\xi_{\mathrm{asx-tx}}^2\right)\\+\xi_{\mathrm{asx-rz}}\left(3\delta\xi_{\mathrm{asx-tx}}^2+175\left(\left(\delta+4\right)t^2-3tw+3w^2\right)\right)\end{array}\right) \tag{B.12}$$

$$0=-\zeta_{\mathrm{amx-tx}}+F_{\mathrm{asx-tx}}+\zeta_{\mathrm{pmx-tx}} \tag{B.13}$$

$$0=-\zeta_{\mathrm{amx-ty}}+F_{\mathrm{asx-ty}}+\zeta_{\mathrm{pmx-ty}} \tag{B.14}$$

$$0=-\zeta_{\mathrm{amx-tz}}+F_{\mathrm{asx-tz}}+\zeta_{\mathrm{pmx-tz}} \tag{B.15}$$

$$0=-\zeta_{\mathrm{amx-rx}}+F_{\mathrm{asx-rx}}+\zeta_{\mathrm{pmx-rx}}+\zeta_{\mathrm{pmx-tz}}\xi_{\mathrm{m-ty}}-\zeta_{\mathrm{pmx-ty}}\xi_{\mathrm{m-tz}} \tag{B.16}$$

$$0=-\zeta_{\mathrm{amx-ry}}+F_{\mathrm{asx-ry}}+\zeta_{\mathrm{pmx-ry}}+\frac{1}{2}w\zeta_{\mathrm{amx-tz}}-w\zeta_{\mathrm{pmx-tz}}+\zeta_{\mathrm{pmx-tz}}\left(\xi_{\mathrm{asx-tx}}-\xi_{\mathrm{m-tx}}-1\right)+\zeta_{\mathrm{pmx-tx}}\xi_{\mathrm{m-tz}} \tag{B.17}$$

$$0=-\zeta_{\mathrm{amx-rz}}+F_{\mathrm{asx-rz}}+\zeta_{\mathrm{pmx-rz}}-\frac{1}{2}w\zeta_{\mathrm{amx-ty}}+w\zeta_{\mathrm{pmx-ty}}+\zeta_{\mathrm{pmx-ty}}\left(-\xi_{\mathrm{asx-tx}}+\xi_{\mathrm{m-tx}}+1\right)-\zeta_{\mathrm{pmx-tx}}\xi_{\mathrm{m-ty}} \tag{B.18}$$

$$\zeta_{\mathrm{pmy-tx}}=\frac{1680\left(5\left(\xi_{\mathrm{m-ty}}-\xi_{\mathrm{asy-tx}}\right)+3\left(\left(\xi_{\mathrm{m-tx}}-\xi_{\mathrm{asy-tz}}\right)^2+\left(\xi_{\mathrm{m-tz}}-\xi_{\mathrm{asy-ty}}\right)^2\right)\right)}{3\left(\xi_{\mathrm{m-tx}}-\xi_{\mathrm{asy-tz}}\right)^2+3\left(\xi_{\mathrm{m-tz}}-\xi_{\mathrm{asy-ty}}\right)^2+175t^2} \tag{B.19}$$

$$\zeta_{\mathrm{pmy-ty}}=\left(48\left(\xi_{\mathrm{m-tz}}-\xi_{\mathrm{asy-ty}}\right)\left(210\left(\xi_{\mathrm{m-ty}}-\xi_{\mathrm{asy-tx}}\right)+129\left(\xi_{\mathrm{m-tx}}-\xi_{\mathrm{asy-tz}}\right)^2+129\left(\xi_{\mathrm{m-tz}}-\xi_{\mathrm{asy-ty}}\right)^2+175t^2\right)\right)/\left(3\left(\xi_{\mathrm{m-tx}}-\xi_{\mathrm{asy-tz}}\right)^2+3\left(\xi_{\mathrm{m-tz}}-\xi_{\mathrm{asy-ty}}\right)^2+175t^2\right) \tag{B.20}$$

$$\zeta_{\mathrm{pmy-tz}}=\left(48\left(\xi_{\mathrm{m-tx}}-\xi_{\mathrm{asy-tz}}\right)\left(210\left(\xi_{\mathrm{m-ty}}-\xi_{\mathrm{asy-tx}}\right)+129\left(\xi_{\mathrm{m-tx}}-\xi_{\mathrm{asy-tz}}\right)^2+129\left(\xi_{\mathrm{m-tz}}-\xi_{\mathrm{asy-ty}}\right)^2+175t^2\right)\right)/\left(3\left(\xi_{\mathrm{m-tx}}-\xi_{\mathrm{asy-tz}}\right)^2+3\left(\xi_{\mathrm{m-tz}}-\xi_{\mathrm{asy-ty}}\right)^2+175t^2\right) \tag{B.21}$$

$$\zeta_{\mathrm{pmy-rx}}=\left(4\left(\begin{array}{l}\delta\left(\xi_{\mathrm{m-ry}}-\xi_{\mathrm{asy-rx}}\right)\left(3\left(\xi_{\mathrm{m-tx}}-\xi_{\mathrm{asy-tz}}\right)^2+3\left(\xi_{\mathrm{m-tz}}-\xi_{\mathrm{asy-ty}}\right)^2+175t^2\right)\\-210\left(5t^2-3tw+3w^2\right)\left(\left(\xi_{\mathrm{m-rx}}-\xi_{\mathrm{asy-rz}}\right)\left(\xi_{\mathrm{m-tx}}-\xi_{\mathrm{asy-tz}}\right)+\left(\xi_{\mathrm{m-rz}}-\xi_{\mathrm{asy-ry}}\right)\left(\xi_{\mathrm{m-tz}}-\xi_{\mathrm{asy-ty}}\right)\right)\end{array}\right)\right)/\left(3\left(\xi_{\mathrm{m-tx}}-\xi_{\mathrm{asy-tz}}\right)^2+3\left(\xi_{\mathrm{m-tz}}-\xi_{\mathrm{asy-ty}}\right)^2+175t^2\right) \tag{B.22}$$

$$\zeta_{\mathrm{pmy-ry}}=4\left(\begin{array}{l}175\left(4t^2-3tw+3w^2\right)\left(\xi_{\mathrm{m-rz}}-\xi_{\mathrm{asy-ry}}\right)\\+6\left(\xi_{\mathrm{m-tx}}-\xi_{\mathrm{asy-tz}}\right)\left(35\left(\xi_{\mathrm{m-ty}}-\xi_{\mathrm{asy-tx}}\right)+24\left(\xi_{\mathrm{m-tx}}-\xi_{\mathrm{asy-tz}}\right)^2+24\left(\xi_{\mathrm{m-tz}}-\xi_{\mathrm{asy-ty}}\right)^2+175t^2\right)\end{array}\right)/\left(3\left(\xi_{\mathrm{m-tx}}-\xi_{\mathrm{asy-tz}}\right)^2+3\left(\xi_{\mathrm{m-tz}}-\xi_{\mathrm{asy-ty}}\right)^2+175t^2\right) \tag{B.23}$$

$$\zeta_{\mathrm{pmy-rz}}=4\left(\begin{array}{l}175\left(4t^2-3tw+3w^2\right)\left(\xi_{\mathrm{m-rx}}-\xi_{\mathrm{asy-rz}}\right)\\-6\left(\xi_{\mathrm{m-tz}}-\xi_{\mathrm{asy-ty}}\right)\left(35\left(\xi_{\mathrm{m-ty}}-\xi_{\mathrm{asy-tx}}\right)+24\left(\xi_{\mathrm{m-tx}}-\xi_{\mathrm{asy-tz}}\right)^2+24\left(\xi_{\mathrm{m-tz}}-\xi_{\mathrm{asy-ty}}\right)^2+175t^2\right)\end{array}\right)/\left(3\left(\xi_{\mathrm{m-tx}}-\xi_{\mathrm{asy-tz}}\right)^2+3\left(\xi_{\mathrm{m-tz}}-\xi_{\mathrm{asy-ty}}\right)^2+175t^2\right) \tag{B.24}$$

$$\zeta_{\mathrm{amy-tx}}=\frac{96\xi_{\mathrm{asy-tx}}\left(35\left(3\left(\xi_{\mathrm{asy-tz}}-\frac{1}{2}w\xi_{\mathrm{asy-ry}}\right)+3\left(\frac{1}{2}w\xi_{\mathrm{asy-rz}}+\xi_{\mathrm{asy-ty}}\right)+5t^2\right)+129\xi_{\mathrm{asy-tx}}^2\right)}{3\xi_{\mathrm{asy-tx}}^2+175t^2} \tag{B.25}$$

$$\zeta_{\mathrm{amy-ty}}=\frac{1}{3\xi_{\mathrm{asy-tx}}^2+175t^2}24\left(\begin{array}{l}w\xi_{\mathrm{asy-rx}}\left(35\left(6\left(\xi_{\mathrm{asy-tz}}-\frac{1}{2}w\xi_{\mathrm{asy-ry}}\right)+5t^2\right)+129\xi_{\mathrm{asy-tx}}^2\right)\\+70\left(\frac{1}{2}w\xi_{\mathrm{asy-rz}}+\xi_{\mathrm{asy-ty}}\right)\left(6\left(\xi_{\mathrm{asy-tz}}-\frac{1}{2}w\xi_{\mathrm{asy-ry}}\right)+5t^2+5\right)+6\xi_{\mathrm{asy-tx}}^2\left(43\left(\frac{1}{2}w\xi_{\mathrm{asy-rz}}+\xi_{\mathrm{asy-ty}}\right)+35\right)\end{array}\right) \tag{B.26}$$

$$\zeta_{\mathrm{amy-tz}}=-\frac{1}{3\xi_{\mathrm{asy-tx}}^2+175t^2}24\left(\begin{array}{l}w\xi_{\mathrm{asy-rx}}\left(35\left(6\left(\frac{1}{2}w\xi_{\mathrm{asy-rz}}+\xi_{\mathrm{asy-ty}}\right)+5t^2\right)+129\xi_{\mathrm{asy-tx}}^2\right)\\-2\left(35\left(\xi_{\mathrm{asy-tz}}-\frac{1}{2}w\xi_{\mathrm{asy-ry}}\right)\left(6\left(\frac{1}{2}w\xi_{\mathrm{asy-rz}}+\xi_{\mathrm{asy-ty}}\right)+5t^2+5\right)+3\xi_{\mathrm{asy-tx}}^2\left(43\left(\xi_{\mathrm{asy-tz}}-\frac{1}{2}w\xi_{\mathrm{asy-ry}}\right)+35\right)\right)\end{array}\right) \tag{B.27}$$

$$\zeta_{\mathrm{amy-rx}}=\frac{1}{3\xi_{\mathrm{asy-tx}}^2+175t^2}4\left(\begin{array}{l}\xi_{\mathrm{asy-rx}}\left(35\left(\begin{array}{l}3w\left(6w+1\right)\left(\xi_{\mathrm{asy-tz}}-\frac{1}{2}w\xi_{\mathrm{asy-ry}}\right)+3w\left(6w+1\right)\left(\frac{1}{2}w\xi_{\mathrm{asy-rz}}+\xi_{\mathrm{asy-ty}}\right)\\+10\left(t^2\left(3w^2+3w+4\right)-3tw+3w^2\right)\end{array}\right)+18w\left(43w+8\right)\xi_{\mathrm{asy-tx}}^2\right)\\+6\left(3\left(43w+8\right)\xi_{\mathrm{asy-tx}}^2+175t^2\left(w+1\right)\right)\left(\frac{1}{2}w\xi_{\mathrm{asy-ry}}+\frac{1}{2}w\xi_{\mathrm{asy-rz}}+\xi_{\mathrm{asy-ty}}-\xi_{\mathrm{asy-tz}}\right)\end{array}\right) \tag{B.28}$$

$$\zeta_{\mathrm{amy-ry}}=-\frac{1}{3\xi_{\mathrm{asy-tx}}^2+175t^2}4\left(\begin{array}{l}6\xi_{\mathrm{asy-tx}}\left(35\left(5t^2-3tw+3w^2\right)\xi_{\mathrm{asy-rx}}+35\left(\left(6w+1\right)\left(\xi_{\mathrm{asy-tz}}-\frac{1}{2}w\xi_{\mathrm{asy-ry}}\right)+5t^2\left(w+1\right)\right)+3\left(43w+8\right)\xi_{\mathrm{asy-tx}}^2\right)\\-\xi_{\mathrm{asy-ry}}\left(3\delta\xi_{\mathrm{asy-tx}}^2+175\left(\left(\delta+4\right)t^2-3tw+3w^2\right)\right)\end{array}\right) \tag{B.29}$$

$$\zeta_{\mathrm{amy-rz}}=\frac{1}{3\xi_{\mathrm{asy-tx}}^2+175t^2}4\left(\begin{array}{l}6\xi_{\mathrm{asy-tx}}\left(-35\left(5t^2-3tw+3w^2\right)\xi_{\mathrm{asy-rx}}+35\left(\left(6w+1\right)\left(\frac{1}{2}w\xi_{\mathrm{asy-rz}}+\xi_{\mathrm{asy-ty}}\right)+5t^2\left(w+1\right)\right)+3\left(43w+8\right)\xi_{\mathrm{asy-tx}}^2\right)\\+\xi_{\mathrm{asy-rz}}\left(3\delta\xi_{\mathrm{asy-tx}}^2+175\left(\left(\delta+4\right)t^2-3tw+3w^2\right)\right)\end{array}\right) \tag{B.30}$$

$$0=-\zeta_{\mathrm{amy-tx}}+F_{\mathrm{asy-tx}}+\zeta_{\mathrm{pmy-tx}} \tag{B.31}$$

$$0=-\zeta_{\mathrm{amy-ty}}+F_{\mathrm{asy-ty}}+\zeta_{\mathrm{pmy-ty}} \tag{B.32}$$

$$0=-\zeta_{\mathrm{amy-tz}}+F_{\mathrm{asy-tz}}+\zeta_{\mathrm{pmy-tz}} \tag{B.33}$$

$$0=-\zeta_{\mathrm{amy-rx}}+F_{\mathrm{asy-rx}}+\zeta_{\mathrm{pmy-rx}}-\zeta_{\mathrm{pmy-ty}}\xi_{\mathrm{m-tx}}+\zeta_{\mathrm{pmy-tz}}\xi_{\mathrm{m-tz}} \tag{B.34}$$

$$0=-\zeta_{\mathrm{amy-ry}}+F_{\mathrm{asy-ry}}+\zeta_{\mathrm{pmy-ry}}+\frac{1}{2}w\zeta_{\mathrm{amy-tz}}-w\zeta_{\mathrm{pmy-tz}}+\zeta_{\mathrm{pmy-tx}}\xi_{\mathrm{m-tx}}+\zeta_{\mathrm{pmy-tz}}\left(\xi_{\mathrm{asy-tx}}-\xi_{\mathrm{m-ty}}-1\right) \tag{B.35}$$

$$0=-\zeta_{\mathrm{amy-rz}}+F_{\mathrm{asy-rz}}+\zeta_{\mathrm{pmy-rz}}-\frac{1}{2}w\zeta_{\mathrm{amy-ty}}+w\zeta_{\mathrm{pmy-ty}}+\zeta_{\mathrm{pmy-ty}}\left(-\xi_{\mathrm{asy-tx}}+\xi_{\mathrm{m-ty}}+1\right)-\zeta_{\mathrm{pmy-tx}}\xi_{\mathrm{m-tz}} \tag{B.36}$$

$$\zeta_{\mathrm{pmz-tx}}=\frac{1680\left(3\left(\left(\xi_{\mathrm{m-tx}}-\xi_{\mathrm{asz-ty}}\right)^2+\left(\xi_{\mathrm{m-ty}}-\xi_{\mathrm{asz-tz}}\right)^2\right)+5\left(\xi_{\mathrm{m-tz}}-\xi_{\mathrm{asz-tx}}\right)\right)}{3\left(\xi_{\mathrm{m-tx}}-\xi_{\mathrm{asz-ty}}\right)^2+3\left(\xi_{\mathrm{m-ty}}-\xi_{\mathrm{asz-tz}}\right)^2+175t^2} \tag{B.37}$$

$$\zeta_{\mathrm{pmz-ty}}=\left(48\left(\xi_{\mathrm{m-tx}}-\xi_{\mathrm{asz-ty}}\right)\left(129\left(\xi_{\mathrm{m-tx}}-\xi_{\mathrm{asz-ty}}\right)^2+210\left(\xi_{\mathrm{m-tz}}-\xi_{\mathrm{asz-tx}}\right)+129\left(\xi_{\mathrm{m-ty}}-\xi_{\mathrm{asz-tz}}\right)^2+175t^2\right)\right)/\left(3\left(\xi_{\mathrm{m-tx}}-\xi_{\mathrm{asz-ty}}\right)^2+3\left(\xi_{\mathrm{m-ty}}-\xi_{\mathrm{asz-tz}}\right)^2+175t^2\right) \tag{B.38}$$

$$\zeta_{\mathrm{pmz-tz}}=\left(48\left(\xi_{\mathrm{m-ty}}-\xi_{\mathrm{asz-tz}}\right)\left(129\left(\xi_{\mathrm{m-tx}}-\xi_{\mathrm{asz-ty}}\right)^2+210\left(\xi_{\mathrm{m-tz}}-\xi_{\mathrm{asz-tx}}\right)+129\left(\xi_{\mathrm{m-ty}}-\xi_{\mathrm{asz-tz}}\right)^2+175t^2\right)\right)/\left(3\left(\xi_{\mathrm{m-tx}}-\xi_{\mathrm{asz-ty}}\right)^2+3\left(\xi_{\mathrm{m-ty}}-\xi_{\mathrm{asz-tz}}\right)^2+175t^2\right) \tag{B.39}$$

$$\zeta_{\mathrm{pmz-rx}}=4\left(\begin{array}{l}\delta\left(\xi_{\mathrm{m-rz}}-\xi_{\mathrm{asz-rx}}\right)\left(3\left(\xi_{\mathrm{m-tx}}-\xi_{\mathrm{asz-ty}}\right)^2+3\left(\xi_{\mathrm{m-ty}}-\xi_{\mathrm{asz-tz}}\right)^2+175t^2\right)\\-210\left(5t^2-3tw+3w^2\right)\left(\left(\xi_{\mathrm{m-rx}}-\xi_{\mathrm{asz-ry}}\right)\left(\xi_{\mathrm{m-tx}}-\xi_{\mathrm{asz-ty}}\right)+\left(\xi_{\mathrm{m-ry}}-\xi_{\mathrm{asz-rz}}\right)\left(\xi_{\mathrm{m-ty}}-\xi_{\mathrm{asz-tz}}\right)\right)\end{array}\right)/\left(3\left(\xi_{\mathrm{m-tx}}-\xi_{\mathrm{asz-ty}}\right)^2+3\left(\xi_{\mathrm{m-ty}}-\xi_{\mathrm{asz-tz}}\right)^2+175t^2\right) \tag{B.40}$$

$$\zeta_{\mathrm{pmz-ry}}=4\left(\begin{array}{l}175\left(4t^2-3tw+3w^2\right)\left(\xi_{\mathrm{m-rx}}-\xi_{\mathrm{asz-ry}}\right)\\+6\left(\xi_{\mathrm{m-ty}}-\xi_{\mathrm{asz-tz}}\right)\left(24\left(\xi_{\mathrm{m-tx}}-\xi_{\mathrm{asz-ty}}\right)^2+35\left(\xi_{\mathrm{m-tz}}-\xi_{\mathrm{asz-tx}}\right)+24\left(\xi_{\mathrm{m-ty}}-\xi_{\mathrm{asz-tz}}\right)^2+175t^2\right)\end{array}\right)/\left(3\left(\xi_{\mathrm{m-tx}}-\xi_{\mathrm{asz-ty}}\right)^2+3\left(\xi_{\mathrm{m-ty}}-\xi_{\mathrm{asz-tz}}\right)^2+175t^2\right) \tag{B.41}$$

$$\zeta_{\mathrm{pmz-rz}}=4\left(\begin{array}{l}175\left(4t^2-3tw+3w^2\right)\left(\xi_{\mathrm{m-ry}}-\xi_{\mathrm{asz-rz}}\right)\\-6\left(\xi_{\mathrm{m-tx}}-\xi_{\mathrm{asz-ty}}\right)\left(24\left(\xi_{\mathrm{m-tx}}-\xi_{\mathrm{asz-ty}}\right)^2+35\left(\xi_{\mathrm{m-tz}}-\xi_{\mathrm{asz-tx}}\right)+24\left(\xi_{\mathrm{m-ty}}-\xi_{\mathrm{asz-tz}}\right)^2+175t^2\right)\end{array}\right)/\left(3\left(\xi_{\mathrm{m-tx}}-\xi_{\mathrm{asz-ty}}\right)^2+3\left(\xi_{\mathrm{m-ty}}-\xi_{\mathrm{asz-tz}}\right)^2+175t^2\right) \tag{B.42}$$

$$\zeta_{\mathrm{amz-tx}}=\frac{96\xi_{\mathrm{asz-tx}}\left(35\left(3\left(\xi_{\mathrm{asz-tz}}-\frac{1}{2}w\xi_{\mathrm{asz-ry}}\right)+3\left(\frac{1}{2}w\xi_{\mathrm{asz-rz}}+\xi_{\mathrm{asz-ty}}\right)+5t^2\right)+129\xi_{\mathrm{asz-tx}}^2\right)}{3\xi_{\mathrm{asz-tx}}^2+175t^2} \tag{B.43}$$

$$\zeta_{\mathrm{amz-ty}}=\frac{1}{3\xi_{\mathrm{asz-tx}}^2+175t^2}24\left(\begin{array}{l}w\xi_{\mathrm{asz-rx}}\left(35\left(6\left(\xi_{\mathrm{asz-tz}}-\frac{1}{2}w\xi_{\mathrm{asz-ry}}\right)+5t^2\right)+129\xi_{\mathrm{asz-tx}}^2\right)\\+70\left(\frac{1}{2}w\xi_{\mathrm{asz-rz}}+\xi_{\mathrm{asz-ty}}\right)\left(6\left(\xi_{\mathrm{asz-tz}}-\frac{1}{2}w\xi_{\mathrm{asz-ry}}\right)+5t^2+5\right)+6\xi_{\mathrm{asz-tx}}^2\left(43\left(\frac{1}{2}w\xi_{\mathrm{asz-rz}}+\xi_{\mathrm{asz-ty}}\right)+35\right)\end{array}\right) \tag{B.44}$$

$$\zeta_{\mathrm{amz-tz}}=-\frac{1}{3\xi_{\mathrm{asz-tx}}^2+175t^2}24\left(\begin{array}{l}w\xi_{\mathrm{asz-rx}}\left(35\left(6\left(\frac{1}{2}w\xi_{\mathrm{asz-rz}}+\xi_{\mathrm{asz-ty}}\right)+5t^2\right)+129\xi_{\mathrm{asz-tx}}^2\right)\\-2\left(35\left(\xi_{\mathrm{asz-tz}}-\frac{1}{2}w\xi_{\mathrm{asz-ry}}\right)\left(6\left(\frac{1}{2}w\xi_{\mathrm{asz-rz}}+\xi_{\mathrm{asz-ty}}\right)+5t^2+5\right)+3\xi_{\mathrm{asz-tx}}^2\left(43\left(\xi_{\mathrm{asz-tz}}-\frac{1}{2}w\xi_{\mathrm{asz-ry}}\right)+35\right)\right)\end{array}\right) \tag{B.45}$$

$$\zeta_{\mathrm{amz-rx}}=\frac{1}{3\xi_{\mathrm{asz-tx}}^2+175t^2}4\left(\begin{array}{l}\xi_{\mathrm{asz-rx}}\left(35\left(\begin{array}{l}3w\left(6w+1\right)\left(\xi_{\mathrm{asz-tz}}-\frac{1}{2}w\xi_{\mathrm{asz-ry}}\right)+3w\left(6w+1\right)\left(\frac{1}{2}w\xi_{\mathrm{asz-rz}}+\xi_{\mathrm{asz-ty}}\right)\\+10\left(t^2\left(3w^2+3w+4\right)-3tw+3w^2\right)\end{array}\right)+18w\left(43w+8\right)\xi_{\mathrm{asz-tx}}^2\right)\\+6\left(3\left(43w+8\right)\xi_{\mathrm{asz-tx}}^2+175t^2\left(w+1\right)\right)\left(\frac{1}{2}w\xi_{\mathrm{asz-ry}}+\frac{1}{2}w\xi_{\mathrm{asz-rz}}+\xi_{\mathrm{asz-ty}}-\xi_{\mathrm{asz-tz}}\right)\end{array}\right) \tag{B.46}$$

$$\zeta_{\mathrm{amz-ry}}=-\frac{1}{3\xi_{\mathrm{asz-tx}}^2+175t^2}4\left(\begin{array}{l}6\xi_{\mathrm{asz-tx}}\left(35\left(5t^2-3tw+3w^2\right)\xi_{\mathrm{asz-rx}}+35\left(\left(6w+1\right)\left(\xi_{\mathrm{asz-tz}}-\frac{1}{2}w\xi_{\mathrm{asz-ry}}\right)+5t^2\left(w+1\right)\right)+3\left(43w+8\right)\xi_{\mathrm{asz-tx}}^2\right)\\-\xi_{\mathrm{asz-ry}}\left(3\delta\xi_{\mathrm{asz-tx}}^2+175\left(\left(\delta+4\right)t^2-3tw+3w^2\right)\right)\end{array}\right) \tag{B.47}$$

$$\zeta_{\mathrm{amz-rz}}=\frac{1}{3\xi_{\mathrm{asz-tx}}^2+175t^2}4\left(\begin{array}{l}6\xi_{\mathrm{asz-tx}}\left(-35\left(5t^2-3tw+3w^2\right)\xi_{\mathrm{asz-rx}}+35\left(\left(6w+1\right)\left(\frac{1}{2}w\xi_{\mathrm{asz-rz}}+\xi_{\mathrm{asz-ty}}\right)+5t^2\left(w+1\right)\right)+3\left(43w+8\right)\xi_{\mathrm{asz-tx}}^2\right)\\+\xi_{\mathrm{asz-rz}}\left(3\delta\xi_{\mathrm{asz-tx}}^2+175\left(\left(\delta+4\right)t^2-3tw+3w^2\right)\right)\end{array}\right) \tag{B.48}$$

$$0=-\zeta_{\mathrm{amz-tx}}+F_{\mathrm{asz-tx}}+\zeta_{\mathrm{pmz-tx}} \tag{B.49}$$

$$0=-\zeta_{\mathrm{amz-ty}}+F_{\mathrm{asz-ty}}+\zeta_{\mathrm{pmz-ty}} \tag{B.50}$$

$$0=-\zeta_{\mathrm{amz-tz}}+F_{\mathrm{asz-tz}}+\zeta_{\mathrm{pmz-tz}} \tag{B.51}$$

$$0=-\zeta_{\mathrm{amz-rx}}+F_{\mathrm{asz-rx}}+\zeta_{\mathrm{pmz-rx}}+\zeta_{\mathrm{pmz-tz}}\xi_{\mathrm{m-tx}}-\zeta_{\mathrm{pmz-ty}}\xi_{\mathrm{m-ty}} \tag{B.52}$$

$$0=-\zeta_{\mathrm{amz-ry}}+F_{\mathrm{asz-ry}}+\zeta_{\mathrm{pmz-ry}}+\frac{1}{2}w\zeta_{\mathrm{amz-tz}}-w\zeta_{\mathrm{pmz-tz}}+\zeta_{\mathrm{pmz-tx}}\xi_{\mathrm{m-ty}}+\zeta_{\mathrm{pmz-tz}}\left(\xi_{\mathrm{asz-tx}}-\xi_{\mathrm{m-tz}}-1\right) \tag{B.53}$$

$$0=-\zeta_{\mathrm{amz-rz}}+F_{\mathrm{asz-rz}}+\zeta_{\mathrm{pmz-rz}}-\frac{1}{2}w\zeta_{\mathrm{amz-ty}}+w\zeta_{\mathrm{pmz-ty}}-\zeta_{\mathrm{pmz-tx}}\xi_{\mathrm{m-tx}}+\zeta_{\mathrm{pmz-ty}}\left(-\xi_{\mathrm{asz-tx}}+\xi_{\mathrm{m-tz}}+1\right) \tag{B.54}$$

$$0=F_{\mathrm{m-tx}}-\zeta_{\mathrm{pmx-tx}}-\zeta_{\mathrm{pmz-ty}}-\zeta_{\mathrm{pmy-tz}} \tag{B.55}$$

$$0=-\zeta_{\mathrm{pmy-tx}}+F_{\mathrm{m-ty}}-\zeta_{\mathrm{pmx-ty}}-\zeta_{\mathrm{pmz-tz}} \tag{B.56}$$

$$0=-\zeta_{\mathrm{pmz-tx}}-\zeta_{\mathrm{pmy-ty}}+F_{\mathrm{m-tz}}-\zeta_{\mathrm{pmx-tz}} \tag{B.57}$$

$$0=F_{\mathrm{m-rx}}-\zeta_{\mathrm{pmx-rx}}-\zeta_{\mathrm{pmz-ry}}-\zeta_{\mathrm{pmy-rz}}-\frac{1}{2}w\zeta_{\mathrm{pmy-tx}}-\frac{1}{2}w\zeta_{\mathrm{pmx-ty}}+\frac{1}{2}w\zeta_{\mathrm{pmy-ty}}-w\zeta_{\mathrm{pmz-tz}} \tag{B.58}$$

$$0=-\zeta_{\mathrm{pmy-rx}}+F_{\mathrm{m-ry}}-\zeta_{\mathrm{pmx-ry}}-\zeta_{\mathrm{pmz-rz}}+\frac{1}{2}w\zeta_{\mathrm{pmx-tx}}+w\zeta_{\mathrm{pmz-ty}}-\frac{1}{2}w\zeta_{\mathrm{pmx-tz}}+\frac{1}{2}w\zeta_{\mathrm{pmy-tz}} \tag{B.59}$$

$$0=-\zeta_{\mathrm{pmz-rx}}-\zeta_{\mathrm{pmy-ry}}+F_{\mathrm{m-rz}}-\zeta_{\mathrm{pmx-rz}}+\frac{1}{2}w\zeta_{\mathrm{pmx-ty}}-\frac{1}{2}w\zeta_{\mathrm{pmy-tz}} \tag{B.60}$$

REFERENCES

[1] R. V. Jones, "Some uses of elasticity in instrument design," *Journal of Scientific instruments*, vol. 39, no. 5, pp. 193, 1962.
[2] R. V. Jones, "Instruments and experiences. Papers on measurement and instrument design," *Wiley Series in Measurement Science and Technology, Chichester, New York: Wiley, 1988*, vol. 1, 1988.
[3] A. G. Erdman, and G. N. Sandor, *Mechanism design (3rd ed.): analysis and synthesis (Vol. 1)*, New Jersey, USA: Prentice-Hall, Inc., 1997.
[4] S. T. Smith, *Flexures: elements of elastic mechanisms*, New York: Gordon and Breach Science Publishers, 2000.
[5] L. L. Howell, *Compliant mechanisms*, New York: John Wiley & Sons, 2001.
[6] N. Lobontiu, *Compliant mechanisms: design of flexure hinges*: CRC press, 2002.
[7] L. L. Howell, *Handbook of compliant mechanisms*, New York: John Wiley & Sons, 2013.
[8] M. L. Culpepper, and G. Anderson, "Design of a low-cost nano-manipulator which utilizes a monolithic, spatial compliant mechanism," *Precision Engineering*, vol. 28, no. 4, pp. 469–482, 2004.
[9] J. J. Gorman, and N. G. Dagalakis, "Force control of linear motor stages for microassembly," in ASME International Mechanical Engineering Conference and Exposition, Washington, D.C., 2003, pp. 615–623.
[10] J. Hesselbach, A. Raatz, and H. Kunzmann, "Performance of pseudo-elastic flexure hinges in parallel robots for micro-assembly tasks," *CIRP Annals - Manufacturing Technology*, vol. 53, no. 1, pp. 329–332, 2004.
[11] D. Kim, D. Y. Lee, and D. G. Gweon, "A new nano-accuracy AFM system for minimizing Abbe errors and the evaluation of its measuring uncertainty," *Ultramicroscopy*, vol. 107, no. 4–5, pp. 322–328, 2007.
[12] S. Kota, J. Joo, Z. Li, S. Rodgers, and J. Sniegowski, "Design of compliant mechanisms: applications to MEMS," *Analog Integrated Circuits and Signal Processing*, vol. 29, no. 1–2, pp. 7–15, 2001/10/01, doi: 10.1023/A:1011265810471, 2001.
[13] G. Schitter, P. J. Thurner, and P. K. Hansma, "Design and input-shaping control of a novel scanner for high-speed atomic force microscopy," *Mechatronics*, vol. 18, pp. 282–288, 2008.
[14] S. Awtar, J. Ustick, and S. Sen, "An XYZ parallel-kinematic flexure mechanism with geometrically decoupled degrees of freedom," *Journal of Mechanisms and Robotics*, vol. 5, no. 1, pp. 015001–015001, doi: 10.1115/1.4007768, 2012.
[15] S. Sen, and S. Awtar, "A closed-form nonlinear model for the constraint characteristics of symmetric spatial beams," *Journal of Mechanical Design*, vol. 135, no. 3, pp. 031003–031003, 10.1115/1.4023157, 2013.
[16] S. Awtar, and A. H. Slocum, "Constraint-based design of parallel kinematic XY flexure mechanisms," *Journal of Mechanical Design*, vol. 129, no. 8, pp. 816–830, doi: 10.1115/1.2735342, 2006.
[17] G. Hao, "Towards the design of monolithic decoupled XYZ compliant parallel mechanisms for multi-function applications," *Mechanical Sciences*, vol. 4, pp. 291–302, 2013.
[18] G. Hao, X. Kong, and R. L. Reuben, "A nonlinear analysis of spatial compliant parallel modules: multi-beam modules," *Mechanism and Machine Theory*, vol. 46, no. 5, pp. 680–706, 2011.
[19] S. Awtar, A. H. Slocum, and E. Sevincer, "Characteristics of beam-based flexure modules," *Journal of Mechanical Design*, vol. 129, no. 6, pp. 625–639, 10.1115/1.2717231, 2006.
[20] G. Hao, and H. Li, "Design of 3-legged XYZ compliant parallel manipulators with minimised parasitic rotations [Online]," *Robotica*, vol. 33, no. 4, pp. 787-806, 2015.
[21] G. Hao, and X. Kong, "Design and modeling of a large-range modular XYZ compliant parallel manipulator using identical spatial modules," *Journal of Mechanisms and Robotics*, vol. 4, no. 2, pp. 021009–021009, 10.1115/1.4006188, 2012.
[22] G. Hao, and X. Kong, "Nonlinear analytical modeling and characteristic analysis of symmetrical wire beam based composite compliant parallel modules for planar motion," *Mechanism and Machine Theory*, vol. 77, no. 0, pp. 122–147, 2014.
[23] L. L. Howell, A. Midha, and T. W. Norton, "Evaluation of equivalent spring stiffness for use in a pseudo-rigid-body model of large-deflection compliant mechanisms," *Journal of Mechanical Design*, vol. 118, no. 1, pp. 126–131, 10.1115/1.2826843, 1996.
[24] G. Chen, and F. Ma, "Kinetostatic modeling of fully compliant bistable mechanisms using timoshenko beam constraint model," *Journal of Mechanical Design*, vol. 137, no. 2, pp. 022301–022301, 10.1115/1.4029024, 2015.
[25] Y. Yue, F. Gao, X. Zhao, and Q. Jeffrey Ge, "Relationship among input-force, payload, stiffness and displacement of a 3-DOF perpendicular parallel micro-manipulator," *Mechanism and Machine Theory*, vol. 45, no. 5, pp. 756–771, 2010.
[26] A. Zhang, and G. Chen, "A comprehensive elliptic integral solution to the large deflection problems of thin beams in compliant mechanisms," *Journal of Mechanisms and Robotics*, vol. 5, no. 2, pp. 021006-021006, 10.1115/1.4023558, 2013.
[27] S. Sen, "Beam constraint model: Generalized nonlinear closed-form modeling of beam flexures for flexure mechanism design," University of Michigan, 2013.
[28] G. Hao, "Extended nonlinear analytical models of compliant parallelogram mechanisms: third-order models," *Transactions of the Canadian Society for Mechanical Engineering*, vol. 39, no. 1, pp. 13, 2015.
[29] S. Awtar, "Synthesis and analysis of parallel kinematic XY flexure mechanisms," PhD thesis, Mechanical Engineering, Massachusetts Institute of Technology, 2003.
[30] H. Li, and G. Hao, "A constraint and position identification (CPI) approach for the synthesis of decoupled spatial translational compliant parallel manipulators," *Mechanism and Machine Theory*, vol. 90, pp. 59–83, 2015.

[31]H. Li, and G. Hao, "Compliant mechanism reconfiguration based on position space concept for reducing parasitic motion," in ASME 2015 International Design Engineering Technical Conferences & Computers and Information in Engineering Conference, Boston, Massachusetts, 2015 pp. V05AT08A004–V05AT08A004.
[32]V. Kumar, J. Schmiedeler, S. V. Sreenivasan, and H.-J. Su, *Advances in mechanisms, robotics and design education and research*: Springer, 2013.
[33]H. Su, D. V. Dorozhkin, and J. M. Vance, "A screw theory approach for the conceptual design of flexible joints for compliant mechanisms," *Journal of Mechanisms and Robotics,* vol. 1, no. 4, pp. 041009, 2009.
[34]H. Su, "Mobility analysis of flexure mechanisms via screw algebra," *Journal of Mechanisms and Robotics,* vol. 3, no. 4, pp. 041010–041010, doi: 10.1115/1.4004910, 2011.
[35]X. Kong, and C. M. Gosselin, *Type synthesis of parallel mechanisms,* Berlin Heidelberg: Springer-Verlag, 2007.
[36]J. Yu, S. Li, H.-j. Su, and M. L. Culpepper, "Screw theory based methodology for the deterministic type synthesis of flexure mechanisms," *Journal of Mechanisms and Robotics,* vol. 3, no. 3, pp. 031008-031008, 10.1115/1.4004123, 2011.
[37]Y. Li, and Q. Xu, "Kinematic analysis and design of a new 3-DOF translational parallel manipulator," *Journal of Mechanical Design,* vol. 128, no. 4, pp. 729-737, 10.1115/1.2198254, 2005.
[38]J. S. Dai, D. Li, Q. Zhang, and G. Jin, "Mobility analysis of a complex structured ball based on mechanism decomposition and equivalent screw system analysis," *Mechanism and Machine Theory,* vol. 39, no. 4, pp. 445-458, 4//, 2004.
[39]J. B. Hopkins, and M. L. Culpepper, "Synthesis of multi-degree of freedom, parallel flexure system concepts via freedom and constraint topology (FACT)-Part I: principles," *Precision Engineering,* vol. 34, no. 2, pp. 259–270, 2010.
[40]J. B. Hopkins, and M. L. Culpepper, "Synthesis of multi-degree of freedom, parallel flexure system concepts via freedom and constraint topology (FACT)-Part II: practice," *Precision Engineering,* vol. 34, no. 2, pp. 271–278, 2010.
[41]J. B. Hopkins, and M. L. Culpepper, "A screw theory basis for quantitative and graphical design tools that define layout of actuators to minimize parasitic errors in parallel flexure systems," *Precision Engineering,* vol. 34, no. 4, pp. 767-776, 10//, 2010.
[42]H. Li, G. Hao, and R. Kavanagh, "Synthesis of decoupled spatial translational compliant parallel mechanisms via freedom and actuation method (FAM)," in ASME 2014 12th Biennial Conference on Engineering Systems Design and Analysis, 2014, pp. V003T17A004–V003T17A004.
[43]J. S. Dai, and J. Rees Jones, "Interrelationship between screw systems and corresponding reciprocal systems and applications," *Mechanism and Machine Theory,* vol. 36, no. 5, pp. 633–651, 2001.
[44]S. Awtar, "Synthesis and analysis of parallel kinematic XY flexure mechanisms," Massachusetts Institute of Technology, Cambridge, MA, 2004.
[45]G. Hao, "Cross-section considerations for wire-beam based translational compliant parallel manipulators," in The 31st International Manufacturing Conference, Cork, Ireland, 2014.

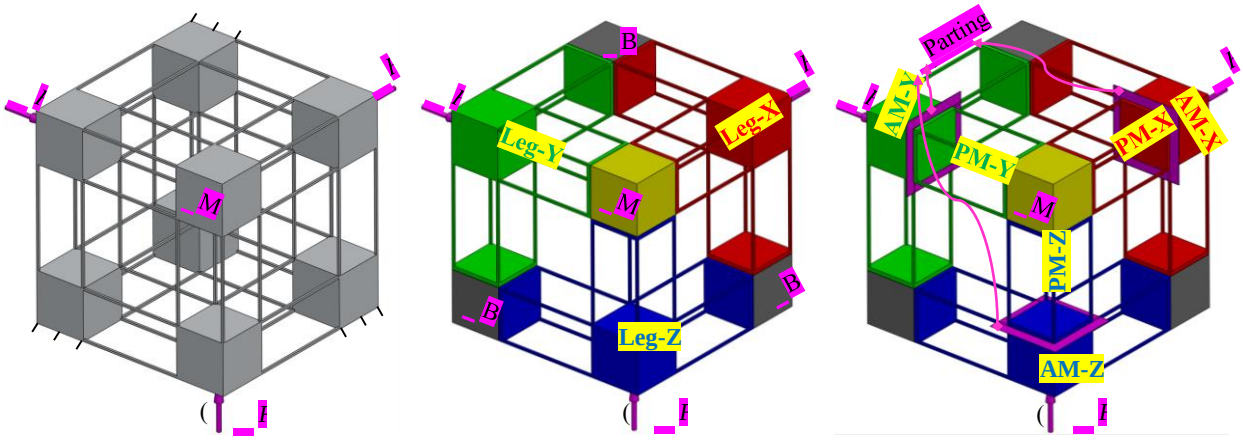

Fig. 1 Decomposition of an XYZ compliant parallel mechanism (CPM): (a) the XYZ CPM, (b) three effective non-basic compliant modules, Leg-X, Leg-Y and Leg-Z, of the XYZ CPM, and (c) non-basic compliant modules, PMs and AMs, of the XYZ CPM (MS and BS represent motion stage and base stage, respectively)

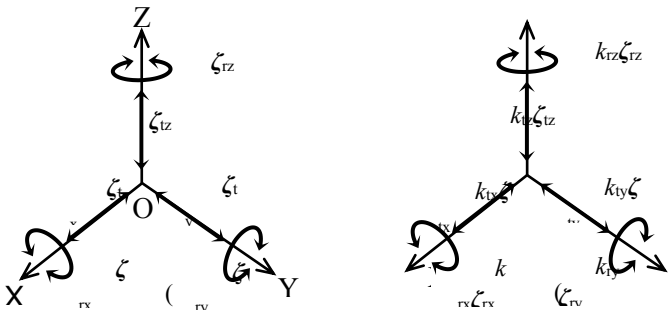

Fig. 2 Principal wrenches and their linear combination in the coordinate system O-XYZ: (a) principal wrenches, and (b) linear combination of the principal wrenches

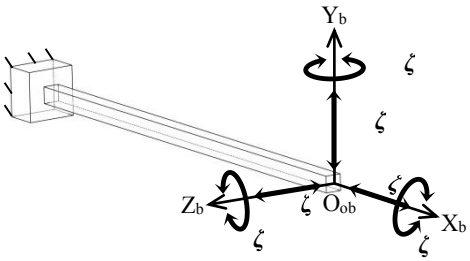

Fig. 3 A wire beam, its local coordinate system and the principal wrenches of the local coordinate system

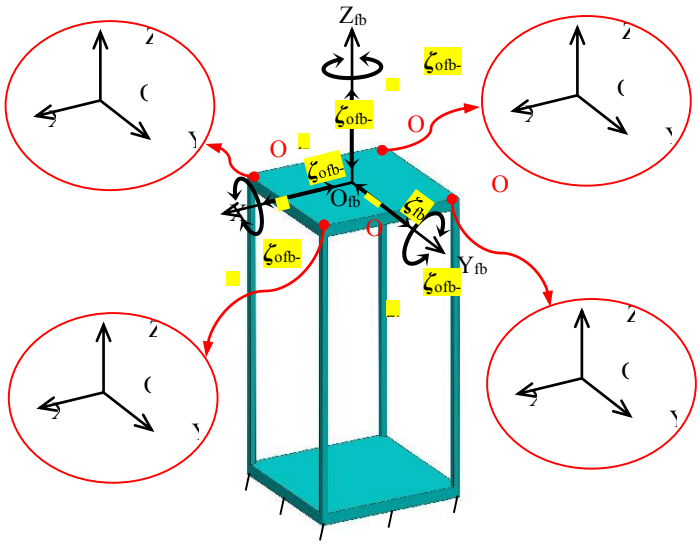

Fig. 4 Illustration of the four-beam non-basic compliant module (or one of the PMs shown in Fig. 1(c)), the global coordinate system O_{fb}-$X_{fb}Y_{fb}Z_{fb}$, and the local coordinate systems O_{fb1}-$X_{fb1}Y_{fb1}Z_{fb1}$, O_{fb2}-$X_{fb2}Y_{fb2}Z_{fb2}$, O_{fb3}-$X_{fb3}Y_{fb3}Z_{fb3}$, O_{fb4}-$X_{fb4}Y_{fb4}Z_{fb4}$

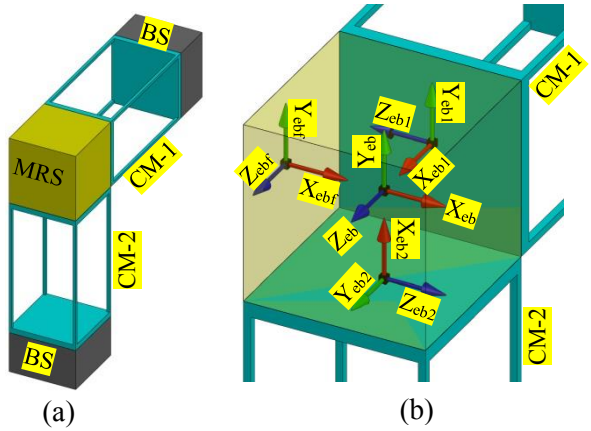

Fig. 5 The decomposition of the eight-beam non-basic compliant module and the defined coordinate systems: (a) the decomposition of the eight-beam non-basic compliant module, and (b) the defined coordinate systems

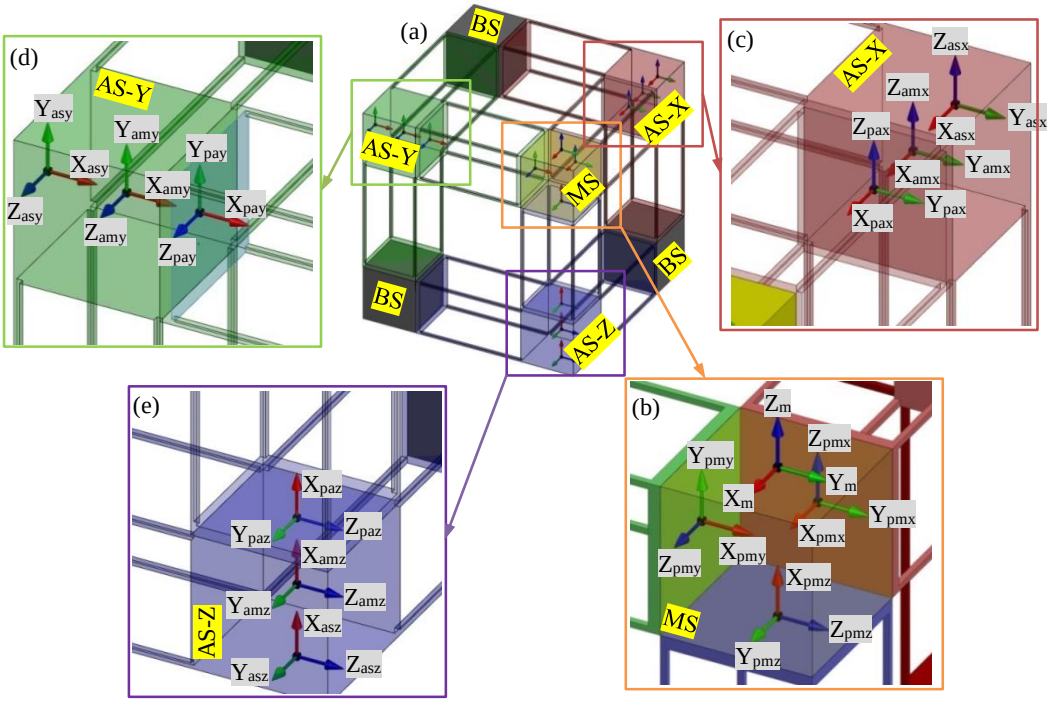

Fig. 6 Coordinate system demonstration: (a) all the coordinate systems; (b) the coordinate systems, O_m-$X_mY_mZ_m$, O_{pmx}-$X_{pmx}Y_{pmx}Z_{pmx}$, O_{pmy}-$X_{pmy}Y_{pmy}Z_{pmy}$ and O_{pmz}-$X_{pmz}Y_{pmz}Z_{pmz}$, fixed on the MS; (c) the coordinate systems, O_{asx}-$X_{asx}Y_{asx}Z_{asx}$, O_{amx}-$X_{amx}Y_{amx}Z_{amx}$ and O_{pax}-$X_{pax}Y_{pax}Z_{pax}$ fixed on the AS-X; (d) the coordinate systems, O_{asy}-$X_{asy}Y_{asy}Z_{asy}$, O_{amy}-$X_{amy}Y_{amy}Z_{amy}$ and O_{pay}-$X_{pay}Y_{pay}Z_{pay}$, fixed on the AS-Y; and (e) the coordinate systems, O_{asz}-$X_{asz}Y_{asz}Z_{asz}$, O_{amz}-$X_{amz}Y_{amz}Z_{amz}$ and O_{paz}-$X_{paz}Y_{paz}Z_{paz}$, fixed on the AS-Z

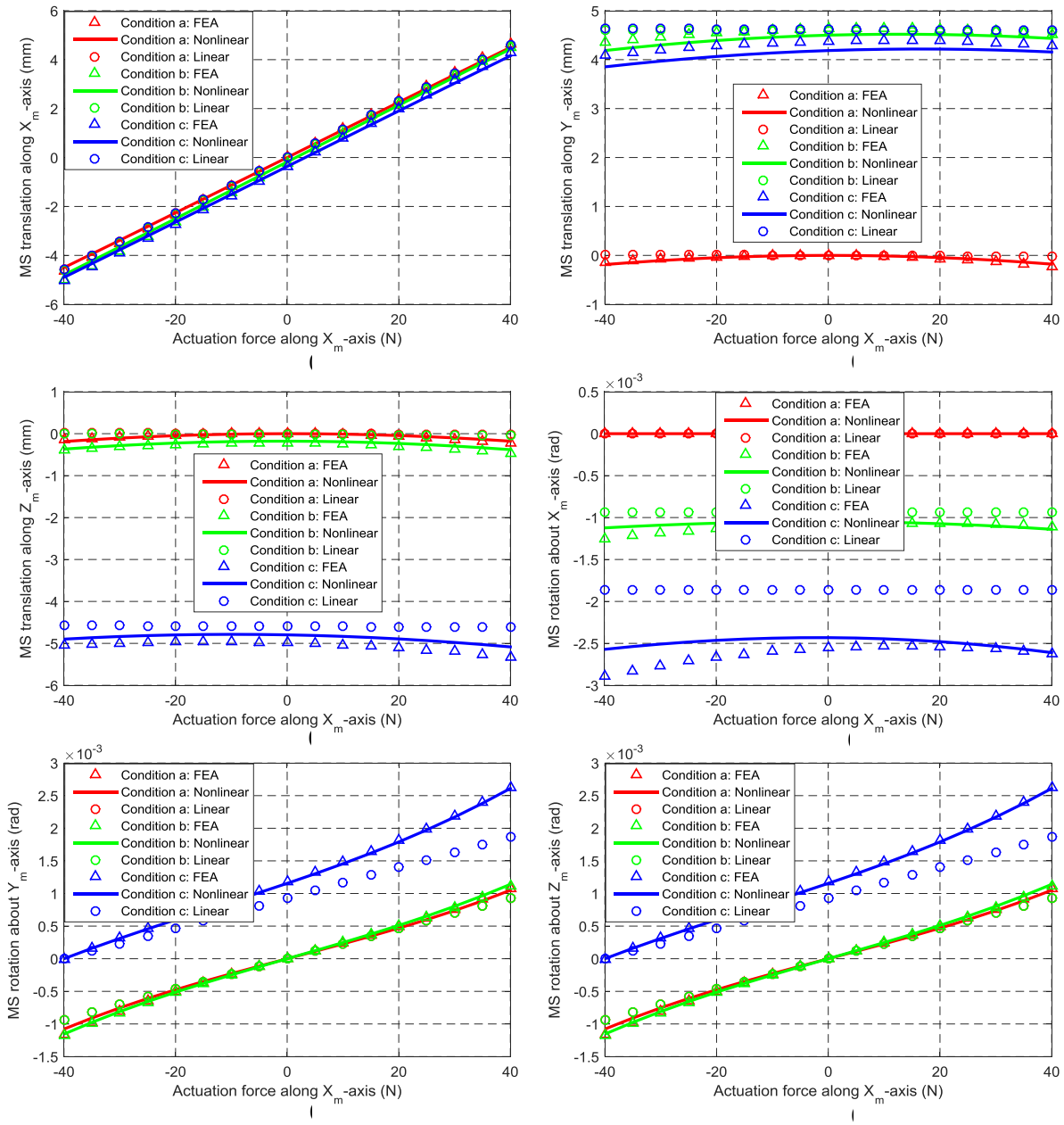

Fig. 7 Comparison of FEA, nonlinear and linear results in terms of the MS's motion: (a) translations along the X_m-axis in the different conditions, (b) translations along the Y_m-axis in the different conditions, (c) translations along the Z_m-axis in the different conditions, (d) rotations about the X_m-axis in the different conditions, (e) rotations about the Y_m-axis in the different conditions, (f) rotations about the Z_m-axis in the different conditions

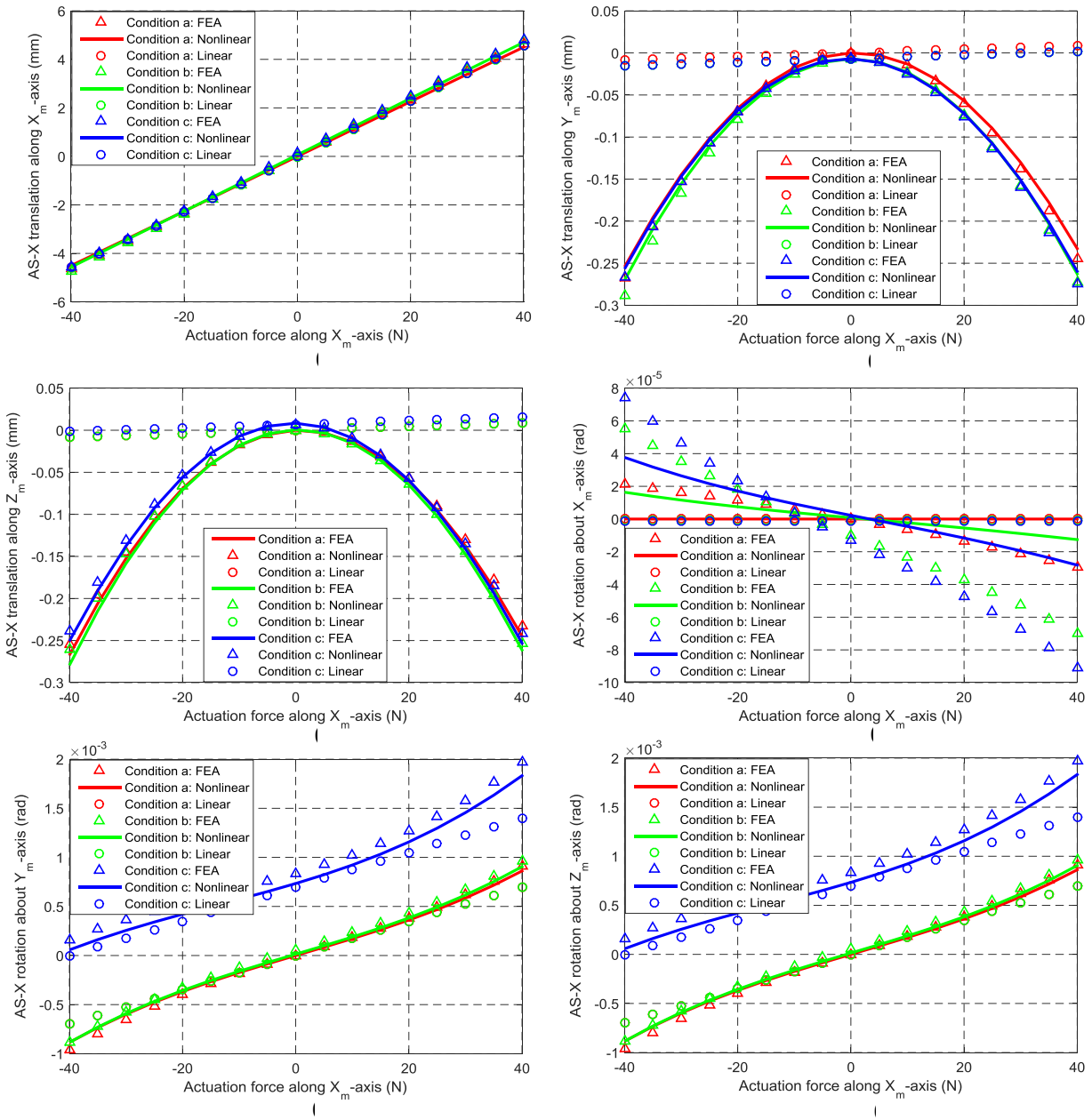

Fig. 8 Comparison of FEA, nonlinear and linear results in terms of the AS-X's motion: (a) translations along the X_m-axis in the different conditions, (b) translations along the Y_m-axis in the different conditions, (c) translations along the Z_m-axis in the different conditions, (d) rotations about the X_m-axis in the different conditions, (e) rotations about the Y_m-axis in the different conditions, (f) rotations about the Z_m-axis in the different conditions

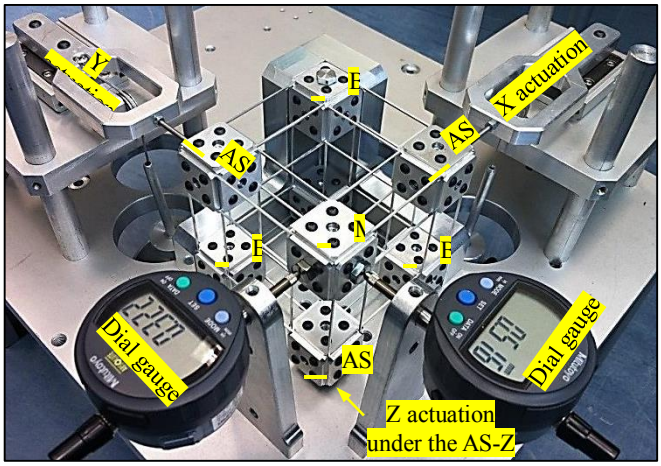

Fig. 9 A prototype of the XYZ CPM with actuation and translational displacement measurement

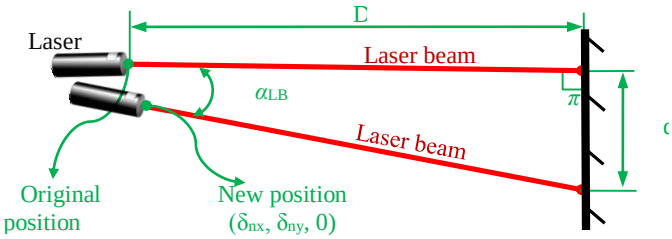

Fig. 10 Principle of measuring the small rotation angle of the MS

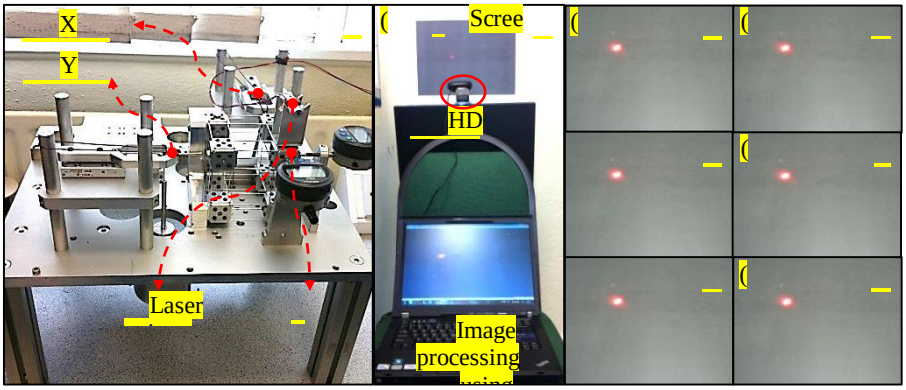

Fig. 11 MS's rotation angle measurement: (a) XYZ CPM experimental test system, (b) screen and image capture facilities, and (c)–(h) captured images of the laser spots at different positions when $f_{asy\text{-}tx}$=0 and $f_{asz\text{-}tx}$=0

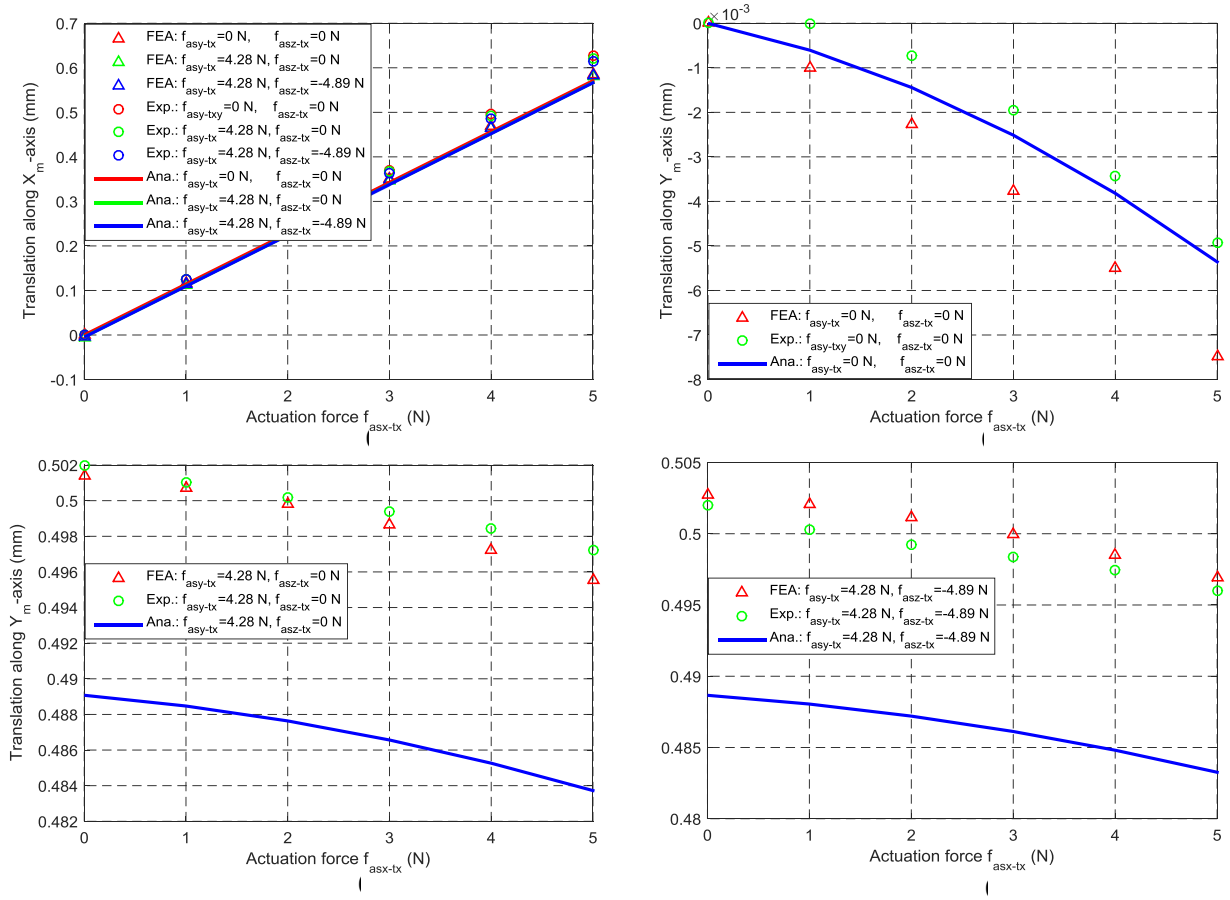

Fig. 12 Comparison of analytical results, FEA results and Experimental results with regard to the translations of the MS along the X- and Y-axes: (a) translations along the X_m-axis in the different conditions, (b) translations along the Y_m-axis when $f_{asy\text{-}tx}$=0 and $f_{asz\text{-}tx}$=0, (c) translations along the Y_m-axis when $f_{asy\text{-}tx}$=4.28N and $f_{asz\text{-}tx}$=0, and (d) translations along the Y_m-axis when $f_{asy\text{-}tx}$=4.28N and $f_{asz\text{-}tx}$=4.89N

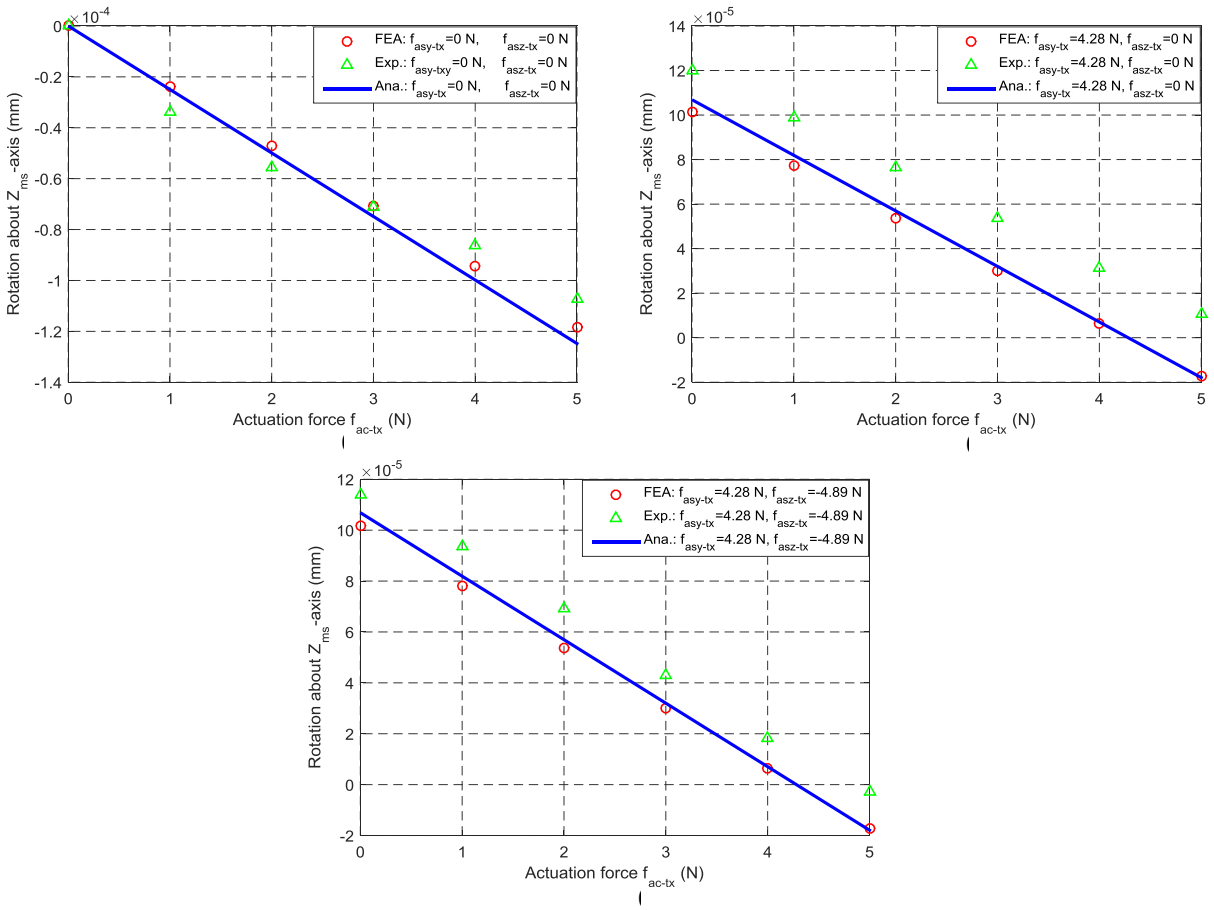

Fig. 13 Comparison of analytical results, FEA results and Experimental results in the different conditions with regard to the rotation of the MS about the Z-axis: (a) when $f_{asy\text{-}tx}$=0 and $f_{asz\text{-}tx}$=0, (b) when $f_{asy\text{-}tx}$=4.28N and $f_{asz\text{-}tx}$=0, and (c) when $f_{asy\text{-}tx}$=4.28N and $f_{asz\text{-}tx}$=4.89N